Nonpremixed and premixed flamelets LES of partially premixed spray flames using a two-phase transport equation of progress variable

Hu, Yong; Kurose, Ryoichi

Combustion and Flame 188 (2018) 227–242

Contents lists available at ScienceDirect

Combustion and Flame

journal homepage: www.elsevier.com/locate/combustflame

Nonpremixed and premixed flamelets LES of partially premixed spray flames using a two-phase transport equation of progress variable

Yong Hu*, Ryoichi Kurose

Department of Mechanical Engineering and Science, Kyoto University, Kyoto daigaku-Katsura, Nishikyo-ku, Kyoto 615–8540, Japan

ARTICLE INFO

Article history:
Received 1 June 2017
Revised 24 July 2017
Accepted 3 October 2017
Available online 5 November 2017

Keywords:
Mixed reaction regime
Large eddy simulation
Flamelet
Spray effect
Reaction progress variable

ABSTRACT

Partially premixed spray flames are simulated with flamelet-based tabulated chemistry parameterized by the mixture fraction and progress variable. The transport equation of the reaction progress variable C is reconsidered, and its formulation for the reacting two-phase flows is derived and employed, which allows the inclusion of spray impacts through a new spray source term that is absent in its gaseous form. Both the nonpremixed and premixed flamelets assuming single reaction regime are implemented in LES, and their validities in spray flames and dependence on the evaporation effect when considering two-phase C equation are examined. The effect of spray, reaction and turbulence interaction is then investigated in comparison with experiments of Sydney reacting acetone sprays, covering the rich, lean and stoichiometric cases. The computed results generally follow the experimental data, but a disagreement between two flamelet simulations is observed especially in rich and lean flames. The premixed flamelets tend to capture the downstream jet spreading while overestimating the peak temperature compared to the nonpremixed chemistry. Flame index analysis indicates that in the present spray flames an evaporation-dominated regime exists inside the upstream core jet and it promotes the coexistence of subsequent interacting premixed and nonpremixed reaction zones, which impedes accurate flame prediction by the single regime flamelets. Furthermore, the spray source term appearing in the derived C equation is identified to act as scalar fluxes driven by sprays in flamelet structures. Including this new source term is found to be important to account for the dissipation effect induced by evaporation on the reaction zone in the flamelet simulation of turbulent spray flames.

1. Introduction

The use of liquid fuel in turbulent combustion is prevalent in many industrial devices. The process in those systems involves complex multi-physics and features interactions among spray evaporation, turbulent transport and vapor fuel/air mixing, as well as chemical reactions that determine the behavior of such combustion devices in relation to both stability and pollutant emissions. Because of the prevaporization effects and dispersion of local fuel droplets, spray flames are often characterized by a partially premixed reaction mode [1,2], exhibiting the properties of both premixed and nonpremixed flames, and show additional evaporation-dependent flame structures compared to pure gas combustion [1,3,4]. Consequently, the increased complexities in reacting sprays make it challenging for simulation, and selecting or developing proper numerical tools for spray combustion modeling is an important issue when the design of more efficient and clean combustion systems is desired.

Large-eddy simulation (LES) has gained increasing attention in recent years and proved its ability to yield reliable computations of complex reacting spray flows [5–10]. Unsteady turbulent structures and mixing are explicitly resolved in LES, but the modeling of subgrid scale (SGS) chemical reactions remains a major issue since the combustion process occurs predominantly in a small scale well below the LES filter width [11]. Several different LES combustion models have been successfully applied in previous spray studies, which are based on either assumed PDF approaches, such as conditional momentum closure [5] and the flamelet approach [6,7], or PDF-like models [12], such as the linear-eddy model [8] and the transported PDF method [9,10]. Among these combustion models, the flamelet-based tabulated chemistry approach shows the most attractive in that with a dramatically reduced computational cost

* Corresponding author.
E-mail address: hu.yong.8m@kyoto-u.ac.jp (Y. Hu).

https://doi.org/10.1016/j.combustflame.2017.10.004

the detailed chemistry can be incorporated in the modeling, which is important to accurately describe the emission formation and transient phenomena highly influenced by the finite-rate chemistry and spray evaporation [13].

For the proper calculations of two-phase flows when using flamelet models, a special care should be paid to the modeling and inclusion of inter-phase couplings [24]. In both nonpremixed and premixed gaseous flamelets modeling, the generated flamelets are usually characterized using two control parameters, the mixture fraction and the reaction progress variable, where the former describes the mixedness of fuel and air, and the latter represents the progress of local reaction. This parameterization of flamelet structures showed its most robust capability in predicting the various flame features [25,26]. In the implementation of flamelet models for turbulent flame simulation, the transport equations of these two control variables are solved together with other flow variables and turbulent effects on the chemistry are accounted for in this manner. The effects, such as the evaporation in spray flames can usually be included in additional source terms of their transport equations. Many studies have been devoted to the examination of the evaporation influence on the mixture fraction field [6,27,28], but few studies have focused on the reaction progress and the spray effects on reaction progress of local mixtures in reacting spray flows.

On the other hand, when applied to the spray flames with mixed interacting combustion regimes, the predictive capabilities of classical flamelet models need to be reconsidered. A turbulent flame in flamelet concept is considered as an ensemble of laminar flames (i.e., the so-called flamelets) [14] and two main strategies to generate the flamelet structures can be found in the literature, which rely on either nonpremixed or premixed flames [15–17]. These two types of flamelet formulations are, therefore, arguably apropos to the description of flames only in the single nonpremixed or premixed burning regime. Recently Knudsen and Pitsch [18] attempted to combine nonpremixed and premixed flamelets in one simulation of an LES spray combustor, where a combustion regime index was used to differentiate the local premixed and diffusion modes of burning. However, this index in its own form presents more complexity and neglects the subfilter contributions where evaporation is significant. Thus, because of the lack of a more reliable flamelet model for spray flames, the classical single flamelet model is still used broadly in studies on reacting spray simulations [6,7,19,20]. EI-Asrag et al. [19] used a nonpremixed flamelet (i.e., the flamelet-progress variable approach) in the large eddy simulation of a lean direct injector combustor to study the emission characteristics. The same flamelet model was adopted by Tachibana et al. [20] in an investigation of combustion instability of a model aircraft combustor. Among recent LES studies, the premixed flamelets were reported in the simulation of the Sydney piloted spray flames [6]. These studies showed that the single flamelet models can somehow reproduce some features of spray flames, but questions still remain regarding to which extent the different single flamelet models can describe the flames at the partially premixed operating conditions and how this would affect the couplings with spray dynamics. Though the performance of different flamelet-based tabulation approaches has been investigated in a few studies of gaseous flames [21,22], it has not been completely identified in the context of spray combustion. Particularly, spray flames feature more complex local flame structures with more distributed and coupled multi-reaction regimes compared to the gaseous counterpart [23].

The main objective of the present work is to identify the spray effects on the reaction progress in the flamelet-based LES modeling and thus, the transport equation of reaction progress variable is reconsidered, and its formulation for two-phase flames is derived. To understand the capabilities and limitations of single-regime flamelets with respect to the prediction of spray flames and their performance with spray impacts when integrating this two-phase transport equation of progress variable, both the nonpremixed and premixed flamelets LES simulations are applied to experimental Sydney partially premixed spray flames with cases featuring various inlet equivalence ratio [29]. The remainder of this paper is organized as follows. The governing equations for gas and liquid phases are introduced in the next section. The emphasis is on the discussion of the derived equation for the progress variable and the closure method for the unclosed terms. Section 3 gives the experimental setup and computational details. The main results and discussion are presented in Section 4, which is followed by the conclusion section.

2. Methodology

2.1. LES governing equations

In the LES of reactive two-phase flows, based on the dilute approximation the filtered conservation equations of gas-phase mass, momentum, and energy, neglecting the volume displacement of dispersed phase, are solved and they are given as

$$\frac{\partial \bar{\rho}}{\partial t} + \frac{\partial (\bar{\rho}\tilde{u}_i)}{\partial x_i} = \bar{\dot{S}}_{\mathrm{v}}, \tag{1}$$

$$\frac{\partial (\bar{\rho}\tilde{u}_j)}{\partial t} + \frac{\partial (\bar{\rho}\tilde{u}_i\tilde{u}_j)}{\partial x_i} = -\frac{\partial \bar{p}}{\partial x_j} + \frac{\partial}{\partial x_i}\left[2\bar{\mu}\left(\tilde{S}_{ij} - \frac{1}{3}\delta_{ij}\tilde{S}_{kk}\right)\right] - \frac{\partial \bar{\tau}_{ij}^{sgs}}{\partial x_i} + \bar{\dot{S}}_{\mathrm{m},j}, \tag{2}$$

$$\frac{\partial (\bar{\rho}\tilde{h})}{\partial t} + \frac{\partial (\bar{\rho}\tilde{u}_i\tilde{h})}{\partial x_i} = \frac{\partial}{\partial x_i}\left(\bar{\rho}\tilde{\alpha}_h\frac{\partial \tilde{h}}{\partial x_i}\right) - \frac{\partial J_h^{sgs}}{\partial x_i} + \bar{\dot{S}}_{\mathrm{e}}. \tag{3}$$

In the above equations, the resolved density-weighted filtered variable is $\tilde{f} = \overline{\rho f}/\bar{\rho}$, and the overbar represents the spatial filtering. $\bar{\rho}$ is the gas density, $\tilde{u}_i$ the velocity, $\bar{p}$ the pressure, $\tilde{S}_{ij}$ the rate-of-strain tensor given by

$$\tilde{S}_{ij} = \frac{1}{2}\left(\frac{\partial \tilde{u}_i}{\partial x_j} + \frac{\partial \tilde{u}_j}{\partial x_i}\right), \tag{4}$$

and the subgrid, unsolved stress $\bar{\tau}_{ij}^{sgs} = \bar{\rho}\widetilde{u_i u_j} - \bar{\rho}\tilde{u}_i\tilde{u}_j$; based on an eddy viscosity assumption, the Smagorinsky model is used to approximate the deviatoric part of this term at the scale of cell width Δ as $\bar{\tau}_{ij}^{sgs} = -2\mu_t\tilde{S}_{ij}$ with $\mu_t = \bar{\rho}(C_s\Delta)^2(2\tilde{S}_{ij}\tilde{S}_{ij})^{1/2}$. Here, the model coefficient C_s is obtained using a dynamic procedure [30]. $\bar{\dot{S}}_{\mathrm{v}}$, $\bar{\dot{S}}_{\mathrm{m},j}$ and $\bar{\dot{S}}_{\mathrm{e}}$ are the source terms for mass, momentum and energy, respectively, accounting for the exchanges between the gas and liquid phases. $\tilde{h}$ is the total enthalpy, and it is included here in order to evaluate the gas-phase temperature that accounts for the spray effect using the correction $\Delta T = (\tilde{h} - h_c)/C_p$[1]. As emphasized by Baba and Kurose [1], the heat loss due to droplet evaporation is relevant in spray flames. The enthalpy h_c taken from flamelet libraries does not include the evaporation effect and a temperature modification should be applied when the enthalpy solved in flowfield outstrips the lower limits of that in flamelet table. The gaseous temperature obtained in this way is also used in the droplet evolution equations. h_c and heat capacity C_p are the tabulated values in the flamelet database introduced below.

In reacting flows, the evolution of reactants and products involved in the chemical reactions are also relevant, and it involves the formation and transportation of thousands of species depending on the fuel considered [12]. A direct solution of the transport

equations for all species is usually not viable in practical 3D combustion simulations. Alternatively, a reduced set of control variables are adopted in a flamelet model to parameterize and tabulate the detailed chemistry database. Usually the mixture fraction Z and progress variable C are selected and their transport equations are solved in conjunction with the flow field. In two-phase flows, the Favre-filtered equation for the mixture fraction can be expressed as,

$$\frac{\partial(\bar{\rho}\tilde{Z})}{\partial t}+\frac{\partial(\bar{\rho}\tilde{u}_i\tilde{Z})}{\partial x_i}=\frac{\partial}{\partial x_i}\left(\bar{\rho}\tilde{\alpha}_Z\frac{\partial\tilde{Z}}{\partial x_i}\right)-\frac{\partial J_Z^{sgs}}{\partial x_i}+\bar{\dot{S}}_v, \tag{5}$$

where the effects of spray evaporation are added in the source term $\bar{\dot{S}}_v$.

The reaction progress variable includes the information of the extent of reaction progress of the reactant mixture. Often, the reacting mixture is described in terms of the mass fraction of major species, the linear combination of which is usually used to define the progress variable [15,16,25]. In this work, according to [31,32], the following formulation of progress variable in a normalized form is chosen

$$C=\frac{Y_c}{Y_c^{eq}}, \tag{6}$$

where Y_c is the sum of CO_2, CO, H_2O and H_2 mass fractions

$$Y_c=Y_{CO_2}+Y_{CO}+Y_{H_2O}+Y_{H_2}, \tag{7}$$

which is consistent with previous studies on hydrocarbon flames [15], and Y_c^{eq} is the chemical equilibrium value of Y_c in the reactant mixture, which depends on the mixture fraction Z. The progress variable C defined by Eq. (6) is in the range of [0, 1], where $C=0$ corresponds to the unburnt mixture and $C=1$ the burnt mixture, and it serves as a useful marker for the description of reaction zone transition in partially premixed combustion [32,33]. Its balance equation for spray flows, as derived in Appendix A, is given as

$$\frac{\partial(\bar{\rho}\tilde{C})}{\partial t}+\frac{\partial(\bar{\rho}\tilde{u}_i\tilde{C})}{\partial x_i}=\frac{\partial}{\partial x_i}\left(\bar{\rho}\tilde{\alpha}_C\frac{\partial\tilde{C}}{\partial x_i}\right)-\frac{\partial J_C^{sgs}}{\partial x_i}+\bar{\bar{\dot{\omega}}}_c+\bar{\dot{S}}_c, \tag{8}$$

$$\bar{\bar{\dot{\omega}}}_c=\bar{\dot{\omega}}_c+\underbrace{C\overline{\frac{1}{Y_c^{eq}}\frac{d^2Y_c^{eq}}{dZ^2}\rho\chi_Z}}_{\omega_{(I)}}+\underbrace{2\overline{\frac{1}{Y_c^{eq}}\frac{dY_c^{eq}}{dZ}\rho\chi_{Z,C}}}_{\omega_{(II)}}, \tag{9}$$

$$\bar{\dot{S}}_c=\overline{-C\frac{1}{Y_c^{eq}}\frac{dY_c^{eq}}{dZ}(\dot{S}_v-Z\dot{S}_v)}, \tag{10}$$

where at the right hand side of Eq. (8), in addition to the diffusion term and chemical reaction term $\bar{\bar{\dot{\omega}}}_c$ that will be encountered in the C equation for gas flames, the last term $\bar{\dot{S}}_c$ is new, and it represents the source term that stems from spray evaporation. The closed forms of these two sources are discussed in the next section. Here, $J_\Phi^{sgs}=\bar{\rho}\widetilde{u_i\Phi}-\bar{\rho}\tilde{u}_i\tilde{\Phi}$ ($\Phi=[h,Z,C]$) is the residual subgrid scalar flux, and it is modeled as

$$J_\Phi^{sgs}=-\bar{\rho}\alpha_{t,\Phi}\frac{\partial\tilde{\Phi}}{\partial x_i}, \tag{11}$$

where the turbulent eddy diffusivity $\alpha_{t,\Phi}$ is determined by $\alpha_{t,\Phi}=\mu_t/(\rho Sc_t)$ with $Sc_t=0.4$ [34]. It is important to note that in addition to the new spray source term appearing in Eq. (8), the unclosed reaction rate includes two more terms $\omega_{(I)}$ and $\omega_{(II)}$ that are associated with the scalar dissipation terms of χ_Z and $\chi_{Z,C}$, which are absent in the fully premixed combustion and represent the contributions from the diffusion mode of burning. Their importance in a liquid-fueled partially premixed case remains to be discussed.

2.2. Closure of reaction rate

The filtered chemical reaction rate in the transport equation of progress variable is obtained by the convolution of the tabulated chemistry database with the probability density function (PDF) to account for the sub-grid turbulent fluctuation effects, which is expressed as

$$\bar{\dot{\omega}}_c=\int_0^1\int_0^1\dot{\omega}_c(Z,C)\tilde{P}(Z,C)dZdC, \tag{12}$$

and

$$\omega_{(I)}=\tilde{C}\bar{\rho}\tilde{\chi}_Z\int_0^1\frac{1}{Y_c^{eq}(Z)}\frac{d^2Y_c^{eq}(Z)}{dZ^2}\tilde{P}(Z)dZ, \tag{13}$$

$$\omega_{(II)}=2\bar{\rho}\tilde{\chi}_{Z,C}\int_0^1\frac{1}{Y_c^{eq}(Z)}\frac{dY_c^{eq}(Z)}{dZ}\tilde{P}(Z)dZ. \tag{14}$$

Here, $\dot{\omega}_c(Z,C)$ is the chemical reaction rate which is read in the flamelet database. $\tilde{P}(Z,C)$ is the joint filtered density function describing the subfilter distribution of the control variables Z and C. The equilibrium value of $Y_c^{eq}(Z)$ is a function of mixture fraction, and it is evaluated in the flamelet tabulation procedure.

The scalar dissipation $\bar{\rho}\tilde{\chi}_Z=\overline{\rho\alpha|\nabla Z|^2}$, decomposed into the resolved and subfilter part χ_Z^{sgs}, is determined in the following manner [35]

$$\bar{\rho}\tilde{\chi}_Z=\bar{\rho}\alpha|\nabla\tilde{Z}|^2+\chi_Z^{sgs}, \tag{15}$$

with

$$\chi_Z^{sgs}=\beta_Z\bar{\rho}\frac{\alpha_t}{\Delta^2}\widetilde{Z''^2}, \tag{16}$$

where $\widetilde{Z''^2}$ is the variance of mixture fraction and β_Z a model constant.

$\bar{\rho}\tilde{\chi}_{Z,C}=\overline{\rho\alpha\nabla Z\cdot\nabla C}$ in Eq. (14) corresponds to the cross-scalar dissipation rate of the mixture fraction Z and progress variable C, and it describes the transport of the reactant mixture across the iso-surface of Z. This term is modeled by the square root of the product of scalar dissipation rates for the mixture fraction $\tilde{\chi}_Z$ and progress variable $\tilde{\chi}_C$, as [32,36]

$$\tilde{\chi}_{Z,C}=\sqrt{\tilde{\chi}_Z\times\tilde{\chi}_C}, \tag{17}$$

where $\tilde{\chi}_C$ is approximated by a commonly used model akin to the formulation of $\tilde{\chi}_Z$ as [37]

$$\bar{\rho}\tilde{\chi}_C=\bar{\rho}\alpha|\nabla\tilde{C}|^2+\chi_C^{sgs}\quad\text{and}\quad\chi_C^{sgs}=\beta_C\bar{\rho}\frac{\alpha_t}{\Delta^2}\widetilde{C''^2}. \tag{18}$$

In Eqs. (16) and (18), the model coefficients β_B and β_C are the time scale ratios and assigned with the value 1.0 [37] in the present study.

2.3. Flamelet modeling

Both nonpremixed and premixed tabulation techniques are used in this work to generate flamelet databases for the prescription of reaction rate described in the above section. The nonpremixed flamelet model assumes the 1D diffusion flame as the basic chemical structure composing the turbulent flames, where the chemical source term is deemed to be mainly balanced by the diffusion processes [14]

$$-\rho\chi_Z\frac{\partial^2Y_i}{\partial Z^2}=\dot{\omega}_{Y_i}. \tag{19}$$

On the other hand, the premixed flamelet structures are obtained by the solution of a laminar steady premixed flame [17]

$$\rho_uS_{l,u}\frac{\partial Y_i}{\partial x}=\frac{\partial(\rho V_{i,x}Y_i)}{\partial x}+\dot{\omega}_{Y_i}. \tag{20}$$

Here, Y_i is the species mass fraction and $\dot{\omega}_{Y_i}$ the corresponding chemical reaction rate. ρ_u and $S_{l,u}$ are the unburnt mixture density and the laminar flame speed, respectively. $V_{i,x}$ denotes the mass diffusion velocity of species i.

In terms of Eq. (19), the diffusion flamelets are calculated with the scalar dissipation rate χ_Z ranging from a very small value to the extinction value, the solution of which would correspond to an S-curve [15]. The steady flamelet structures together with the unstable flamelet solutions along this curve are then tabulated in a table lookup parameterized by the mixture fraction and progress variable. On the other hand, the premixed flamelet table consists of premixed flame structures generated by means of Eq. (20) with various initial fuel/air mixing states.

For application to the LES simulation, the generated flamelet databases need to be formulated to the Favre-filtered quantities by integrating the joint PDF $\tilde{P}(Z,C)$. In the widely used presumed PDF modeling [6,7,12], under the assumption of statistical independence, the joint PDF is often expressed as the product of the marginal PDF of the dependent variables, $\tilde{P}(Z,C)=\tilde{P}(Z)\tilde{P}(C)$.

In this study, the presumed PDF method is adopted with a beta-PDF distribution for Z and a delta function for C in nonpremixed flamelet modeling as

$$\tilde{\psi}=\int_0^1 \psi\tilde{P}\left(Z;\tilde{Z},\widetilde{Z''^2},\tilde{C}\right)dZ, \tag{21}$$

and with a beta PDF describing the distribution of C and delta function for the Z in premixed flamelet modeling

$$\tilde{\psi}=\int_0^1 \psi\tilde{P}\left(C;\tilde{C},\widetilde{C''^2},\tilde{Z}\right)dC, \tag{22}$$

where ψ denotes the reaction rate and species mass fraction that are obtained from the flamelet tables. $\widetilde{Z''^2}$ and $\widetilde{C''^2}$ are the filtered variance of mixture fraction and progress variable, respectively, and used in the evaluation of the beta PDF distribution. They are determined in the LES calculation by their algebraic model

$$\widetilde{\Psi''^2}=\beta_v\Delta^2\left(\frac{\partial\tilde{\Psi}}{\partial x_i}\right)^2 \tag{23}$$

with the model constant β_v set to 0.15 according to [6,39,40]

It is worth mentioning that the combination of flamelet models with the transported PDF method is another reliable alternative approach in spray combustion simulations [26,41] that avoids the statistical independence assumption for the joint PDF and directly solves the transport equation of joint PDF of the mixture fraction and other considered control variables, although additional computational cost may arise due to the solution of high-dimensional PDF transport equation. This approach is outside the scope of this study, and the reader can refer to Ref. [42] for more information.

2.4. Sub-models for liquid phase

The liquid phase is assumed to be dilute spray consisting of spherical single-component droplets. The droplet coalescence or breakup is not considered. The dilute spray evolves according to a set of Lagrangian equations describing the dynamics of fuel droplets including their temperature, T_d, mass, m_d, velocity, $\mathbf{v}_d$, and trajectory, $\mathbf{x}_d$, in the continuous gas phase. With the assumption of heavy particles, the forces considered to have a significant contribution to the droplets motion include the drag force, gravitational force and a random force due to the subgrid fluctuations in LES

$$d\mathbf{x}_d=\mathbf{v}_d dt, \tag{24}$$

$$d\mathbf{v}_d=\left(\frac{\tilde{\mathbf{u}}-\mathbf{v}_d}{\tau_d}\right)dt+\mathbf{g}dt+\left(\frac{C_0k^{sgs}}{\tau_c}\right)^{1/2}d\mathbf{W}, \tag{25}$$

$$dT_d=\frac{Nu}{3Pr}\left(\frac{c_{p,g}}{c_{p,l}}\right)\frac{f_2\left(\tilde{T}-T_d\right)}{\tau_d^{St}}dt+\frac{L_V}{c_{p,l}}\left(\frac{dm_d}{m_d}\right), \tag{26}$$

$$dm_d=-\frac{m_d}{\tau_d^{St}}\left(\frac{Sh}{3Sc}\right)\ln(1+B_M)dt. \tag{27}$$

Here, $\tilde{\mathbf{u}}$, and $\tilde{T}$ are the local gas properties, namely gas velocity and temperature, respectively, at the droplet position. L_V is the latent heat of evaporation, $\mathbf{g}$ the gravitational acceleration, $c_{p,g}$ and $c_{p,l}$ the specific heat capacities of the gas and liquid phase, Nu and Sh the Nusselt number and Sherwood number. $\tau_d^{St}=2\rho_l r_d^2/(9\mu)$ the particle relaxation time in Stokes regime. f_2 is the correction factor for the interphase thermal transfer of evaporating droplets [43]. $k^{sgs}=C_s^{-\frac{8}{3}}(\frac{\mu_t}{\rho\Delta})^2$ is the subgrid kinetic energy and $C_0=1$ [44]. $d\mathbf{W}$ denotes the increment of a stochastic Wiener process. τ_d is the particle kinetic response time and can be expressed as

$$\tau_d=\frac{8}{3}\frac{\rho_l}{\rho_g}\frac{r_d}{C_D|\tilde{\mathbf{u}}-\mathbf{v}_d|}, \tag{28}$$

where r_d is the particle radius, ρ_g the gas density, ρ_l the density of droplets and C_D the drag coefficient given by an empirical expression [1]

$$C_D=\frac{24}{Re_d}\left[\frac{1+0.0545Re_d+0.1Re_d^{0.5}(1-0.03Re_d)}{1+b|Re_b|^c}\right], \tag{29}$$

$$\begin{aligned} b&=0.06+0.077e^{(-0.4Re_d)}\\ c&=0.4+0.77e^{(-0.04Re_d)}\end{aligned} \tag{30}$$

in which $Re_d=2\rho_g r_d u_{sl}/\mu$ and Re_b denote the droplet Reynolds numbers based on the slip velocity $u_{sl}=|\tilde{\mathbf{u}}-\mathbf{v}_d|$ and the blowing velocity $u_b=\frac{dm_d}{dt}(4\pi r_d^2\rho_g)^{-1}$, respectively.

According to [44], τ_c denotes a typical timescale for the interactions between the particle and turbulence, and it is evaluated with

$$\tau_c=\tau_d^{2a}\left(\frac{\Delta}{\sqrt{k^{sgs}}}\right)^{1-2a},\quad \text{and}\quad a=0.8. \tag{31}$$

The mass transfer number B_M is the normalized fuel flux around the droplet surface, which involves the fuel mass fraction in surrounding gas $\tilde{Y}_F$ and that at the droplet surface $Y_{F,s}$

$$B_M=\frac{Y_{F,s}-\tilde{Y}_F}{1-Y_{F,s}} \tag{32}$$

with $Y_{F,s}$ determined by the Clausius–Clapeyron relation [1,45].

Additionally, studies have shown the important effects of SGS scalar fluctuations in the modeling of spray properties, including auto-ignition [46]. In this study, we adopt a technique in the framework of flamelet modeling that uses the subfilter presumed PDF to prescribe random gas quantities of $\tilde{Y}_F$ and $\tilde{T}$ for the evaporating droplets [28]. In this algorithm, the pairing procedure of the droplets with a stochastic value of $\tilde{Y}_F$ or $\tilde{T}$ is reinitiated after an intermittent coupling process, which was set based on the SGS turbulence timescale, $\tau_t=\frac{\Delta^2}{\max(\alpha,\alpha_t)}$, as applied in the study of De and Kim [28]. In this work, a time of $\min(\tau_t,\tau_c)$ is used instead to ensure the droplet/gas subfilter correlation is renewed when the droplet breaks away from an eddy or the eddy is dissipated, and to numerically avoid the appearance of spurious long-duration correlation.

2.5. Spray source terms

The spray source terms in the gas-phase governing equations account for the two-phase coupling through heat and mass transfers. By using the particle-source-in-cell (PSI-Cell) method [1], the

mass, momentum, and energy exchange terms, which are $\bar{\dot{S}}_v$, $\bar{\dot{S}}_m$, and $\bar{\dot{S}}_e$, respectively, in Eqs. (1)–(3) are expressed as

$$\bar{\dot{S}}_v = -\frac{1}{\Delta V}\sum_{k=1}^{N_d} n_{d,k}\frac{d}{dt}\left(m_{d,k}\right) \tag{33}$$

$$\bar{\dot{S}}_m = -\frac{1}{\Delta V}\sum_{k=1}^{N_d} n_{d,k}\frac{d}{dt}\left(m_{d,k}\mathbf{v}_{d,k}\right) \tag{34}$$

$$\bar{\dot{S}}_e = -\frac{1}{\Delta V}\sum_{k=1}^{N_d} n_{d,k}\left[\frac{1}{2}\frac{d}{dt}\left(m_{d,k}\mathbf{v}_{d,k}^2\right) + \frac{d}{dt}\left(m_{d,k}c_{p,l}T_{d,k}\right)\right] \tag{35}$$

where the spray source terms in each cell volume ΔV are obtained from the summation of all the droplet parcels located within this cell. Droplet groupings are used, and $n_{d,k}$ represents the number of real fuel droplets in one computational parcel k.

The source term $\bar{\dot{S}}_c$ appearing in the newly derived C equation (8) can be obtained with

$$\bar{\dot{S}}_c = -\tilde{C}\left(\bar{\dot{S}}_v - \tilde{Z}\bar{\dot{S}}_v\right)\int_0^1 \frac{1}{Y_c^{eq}(Z)}\frac{dY_c^{eq}(Z)}{dZ}\tilde{P}(Z)dZ, \tag{36}$$

neglecting the higher-order correlations in the spray source, mixture fraction and progress variable field.

3. Flame configuration and computation details

3.1. Test cases

The flames considered in the present LES computations are the piloted turbulent spray flames, which were experimentally studied at the University of Sydney [29]. This Sydney piloted spray burner bears an open annular configuration and is well designed to be representative of reactive spray flows stabilized by hot gaseous mixtures that are widely encountered in real engine applications. The burner geometry comprises a central spray jet along with a mixture of prevaporized fuel and air, surrounding which is an annulus of outer diameter 25 mm supplying the hot-pilot stream for the stabilization of the main jet. A stoichiometric mixture of acetylene, hydrogen and air is maintained for the pilot flow. The spray is generated by an ultrasonic nebulizer placed 215 mm upstream of the jet exit plane, and the central nozzle diameter $D = 10.5$ mm. Moreover, there is an air co-flow with a diameter of 104 mm and bulk velocity of 4.5 m/s. A series of cases involving nonreacting and reacting sprays with acetone and ethanol fuel droplets have been investigated with this burner, of which three with acetone fuel are simulated in this work. They are referred to as AcF3, AcF4 and AcF6, which feature the rich, lean and stoichiometric operating condition, respectively.

3.2. Computational methods and boundary conditions

A sketch of the computational domain is presented in Fig. 1. The simulations are performed using an in-house LES code FK^3 [1,47,48] with the finite difference formulation in a Cartesian coordinate system. The spatial gradients in the momentum equation are approximated with a fourth-order central difference scheme, and a WENO scheme is used for the discretization of nonlinear terms in the scalars' governing equations. The time integration is based on a third-order explicit Runge–Kutta method. The computational domain extends to 48D × 11D × 11D in three directions and consists of around 5 M grid points with finer meshes near the inlet and shear layer. The diffusion and premixed flamelet libraries for acetone/air combustion are generated using the configurations of a 1D counterflow diffusion flame and a premixed freely propagating flame, respectively, with the FlameMaster code [38].

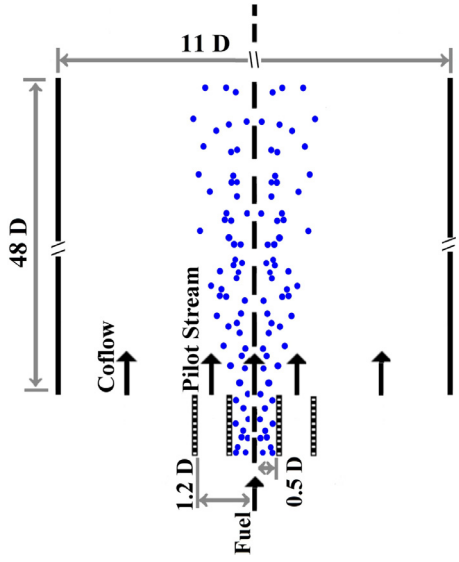

Fig. 1. Sketch of the computational domain. .

In flamelet equations, the boundary conditions at $Z = 1$ and $Z = 0$ are set as pure fuel acetone and air at temperature of 300 K. A detailed reaction mechanism with 83 species and 419 element reactions, developed by Pichon et al. [49] is used to model the acetone oxidation. The stoichiometric mixture fraction Z_{st} is 0.095. The diffusion flamelet solutions comprise the solutions with the scalar dissipation rate varying from 0.1×10^{-2}/s to the extinction value of 102/s, resulting in a total of 126 different steady and unsteady flamelet solutions. The flammable region in the premixed acetone flame calculation is in the equivalence ratio range of (0.39, 2.55), and a linearly interpolated mixing state is applied outside this flammability limit. It is noteworthy that in case of occurrence of envelope flame, where chemical reaction can happen around each droplets, this mixing assumption might be violated for the mixture at the lean side [50] due to the increased temperature and species gradient in the gas area around this envelope flame. But in both the experimental and computational studies of present dilute spray flames [28,29], there is no clear indication of the existence of envelope flame, which is thus assumed to be negligible and not considered in the present study.

The boundary data of the gas phase and liquid phase at the first experimental cross-section are used to determine the inlet computational profiles. A digital filter technique is employed to generate the pseudo-turbulence for the jet velocities at inlet based on the method proposed by Klein et al. [51]. The progress variable in the pilot-stream is set to unity and zero for other inlet boundaries. The inlet liquid particles are randomly distributed around each grid point, and the droplet size is assigned with the Rosin–Rammler distribution, matching the measured Sauter mean diameter. The droplet grouping is used depending on the size, and for each size group, particle velocity is assigned based on the velocity distribution of specific size class given by experiments. The number of droplets within each parcel is determined such that the measured liquid fuel mass flow rate is preserved. The number of droplet parcels in the computational domain remains around 6.5×10^5, and a few cases with higher and lower particle numbers have been studied to ensure the suitability of the particle number used in the present computations. The statistics are collected for each case over eight flow-through times, and all simulations are performed using CRAY: XE6 at the ACCMS, Kyoto University with 576 cores and approximately 100 h of wall clock time.

Table 1
Experimental inlet conditions of acetone fuel spray flames, AcF3, AcF4 and AcF6, experimental set B [29].

Test Case	AcF3	AcF4	AcF6
Bulk jet velocity (m/s)	24	24	36
Hot-pilot stream velocity (m/s)	11.4	11.4	11.4
Bulk co-flow velocity (m/s)	4.5	4.5	4.5
Air carrier flow-rate (g/min)	150	150	225
Liquid fuel flow-rate (g/min)	19.4	10.4	21.6
Vapor fuel flow-rate (g/min)	25.7	13.0	23.4
Equivalence ratio	1.6	0.8	1.0

The inlet boundary conditions for the three cases of reacting acetone spray (AcF3, AcF4 and AcF6) are listed in Table 1.

4. Results

4.1. Spray flames calculated with different flamelet databases

Partially premixed acetone spray flames have been simulated and the acetone/air combustion is described with the tabulated detailed chemistry by counterflow diffusion flamelet and premixed flamelet, respectively. The Sydney spray flames characterized by different rates of pre-vaporization, covering cases of rich (AcF3), lean (AcF4), and stoichiometric (AcF6) premixing mixtures at inlet, are considered with an attempt to thoroughly examine the performance of different tabulated chemistries and the effects on spray dynamics.

4.1.1. Gas temperature

Figure 2 shows the snapshots of the instantaneous gas-phase temperature for spray flames of AcF3, AcF4 and AcF6, where for each case the figures at the left and right hand side correspond to the results from the nonpremixed and premixed flamelet calculations, respectively. By comparing three flame cases, it can be seen that the computed temperature in the premixed and nonpremixed cases differ from each other, especially near the center part of the jet. The diffusion flamelet (left-side figure for each case) computes an earlier combustion with the center flame front established closer to the nozzle exit, and comparatively, this inner flame brush is anchored further downstream in the simulations with premixed flamelets (right-side figure in each case). This is particularly evident in the rich case of spray flame AcF3. Meanwhile, it can be observed that this center high-temperature reaction zone initiates earlier in the lean spray flame AcF4 than in AcF3 or the stoichiometric case AcF6, which has the most reactive mixture at the inlet. The reason for this will be discussed in the subsequent section. Since the injected fuel droplets move towards this inner flame front, the predicted distinct temperature is expected to affect the spray evaporation, the statistics of which will be discussed in Section 4.1.2.

With the general idea obtained from the above comparison, Fig. 3 compares the experimental measurements with the radial profiles of mean gas temperature at different axial locations $x/D =$ 10, 20, and 30, computed using nonpremixed and premixed flamelets for three flame cases. Overall, the trends of changes that the experimental values suggest towards the downstream of the jet are captured by two flamelet model computations. In the three cases, at the jet exit spray flames are characterized by the partially premixed vapor fuel/air mixtures at the ambient temperature. When injected into the combustion field, this center jet mixture together with fuel droplets is sheathed by the pilot flame, and due to the high initial momentum of the jet carrier, the immediate inward propagation of the hot-pilot stream is retarded. However, when moving downstream away from the nozzle exit, because of the turbulent mixing and droplet evaporation, the main jet is slowly heated up, as evidenced by the increasing values of gas temperature near the centerline indicated by the experiments and both nonpremixed and premixed computations. In comparison, a marked difference is found in the predictions by the two flamelet databases. The nonpremixed flamelet predicts a higher temperature compared to the premixed flamelet, indicating the important influence of turbulence/chemistry interactions on the inner flame propagating. In general, the premixed flamelet shows a better result in capturing the flame spreading in the radial direction towards the downstream locations.

Additionally, it is observed that, near the flame edge of the radial position $r/D = 1$, where the stoichiometric mixtures are located, the premixed flamelet slightly overestimates the peak temperature. As pointed out by Ramaekers et al. [22] in the study of different flamelet models for the simulations of Sandia flames, the difference between flamelets in the species mass fraction

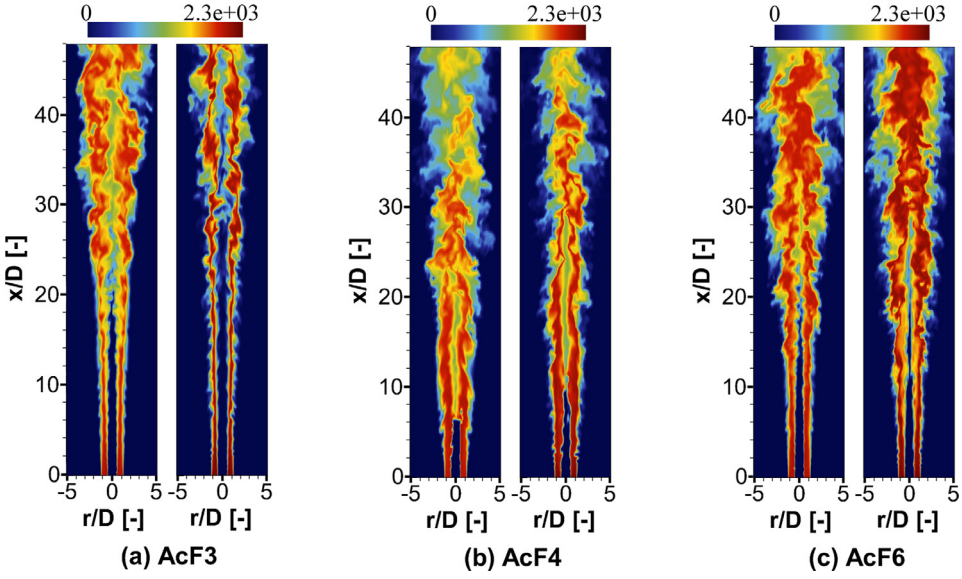

Fig. 2. Representative instantaneous filtered gas temperature for spray flame AcF3, AcF4 and AcF6, where the predicted results from nonpremixed and premixed flamelet models are presented at left and right hand side, respectively, for each case.

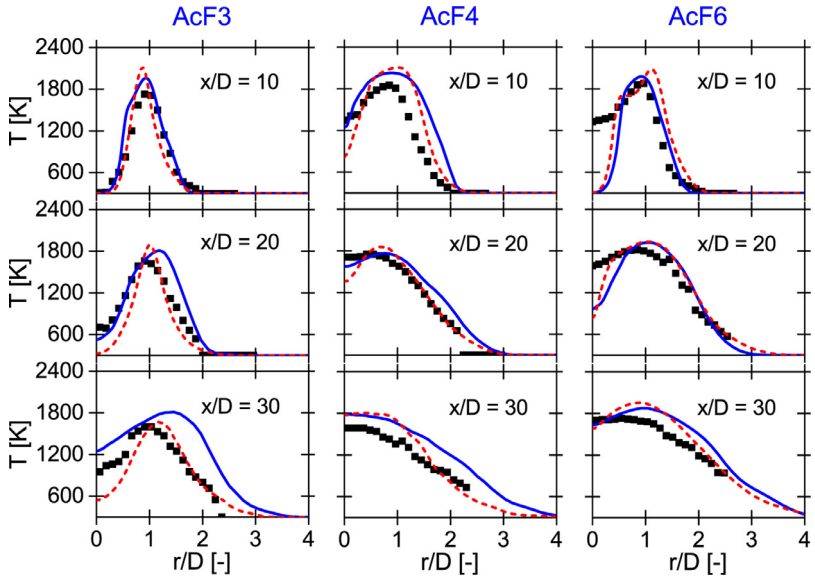

Fig. 3. Comparison of radial distribution of mean gas temperature profile predicted by nonpremixed and premixed flamelet database for spray flames AcF3 (left), AcF4 (middle) and AcF6 (right) at three downstream locations of $x/D = 10$, 20, and 30. Solid line: nonpremixed flamelet calculations; Short dash: premixed flamelet calculations; Filled dots: experimental data [29].

predictions can be attributed to the fact that in the nonpremixed flamelet, species are transported between the iso-mixture fraction line passing through the Z_{st} plane where intense reaction occurs, while they only diffuse in the C-direction in premixed flamelets. This can be used to explain the overestimated peak of flame temperature in premixed flamelet modeling. The diffusion of heat from the reaction zone ($Z = Z_{st}$) to the surrounding mixtures is guaranteed in diffusion flamelets.

Furthermore, note that, in AcF6, although reasonable agreement with the experimental data is observed for the predictions at the downstream locations, a considerable underprediction of gas temperature near the centerline by both the nonpremixed and premixed simulations is found at the upstream cross-section $x/D = 10$. Similar disagreements have been reported in other studies [5,39,40]. It was argued that this deviation from the experimental data can arise from the uncertainty in the measurements. In the experiments, the gas-phase temperature was measured using thermocouples, which can lead to significant errors in the high temperature zone of two-phase flows.

4.1.2. Spray statistics

In this section, the influences of diffusion and premixed flamelet calculations on the droplet properties, namely evaporation and dispersion, are studied in comparison with the available experimental data [29].

In Fig. 4, the computed radial profiles of droplet Sauter mean diameter (SMD) at four different cross-sections $x/D = 5$, 10, 20, and 30 are compared with experimental data. In the two different flamelet modelings, the simulated values generally follow the measured profiles of droplet SMD in all three cases, although an overestimated SMD is obtained by both flamelets in the simulations of spray AcF4 for the cross-sections $x/D > 10$. These higher values can be attributed to the overpredicted gas-phase temperature seen in Fig. 3 for AcF4 at $x/D = 10$. Similar apparent discrepancies are also observed in AcF3 at $x/D = 30$, where the nonpremixed flamelet yields a much larger SMD than both the premixed flamelet and measurements, and this is consistent with the noted disparity in temperature profiles shown at the same location in Fig. 3. This observed concordance between the predicted SMD and temperature can be due to the poly-dispersity of present spray flames. A wide range of droplets differing in size and dynamic history dictate the injected sprays, within which the small droplets tend to evaporate faster and are more likely affected by the gas temperature. Comparatively, the larger droplets can survive far downstream, and more time is needed for heating up the large droplets because of the size dependence of relaxation time [26]. Also, it is noted that, when approaching the flame region $0.4 < r/D < 0.8$ (the shear layer between the main jet and pilot flame), the predictions yield a slightly higher SMD compared to the measured data, which suggests the droplets on the jet edge evaporate more rapidly than those in the inner region of the spray.

Figure 5 shows the radial profiles of the axial mean, U_d and fluctuating, U_d'' velocities of droplets at four cross sections. Generally, the computations show good agreement with measurements. The calculated mean droplet axial velocities from flamelet models well capture the trend of droplet dispersion when traveling far away from the jet exit, but a distinguishable disagreement between the two flamelet predictions is found. This can be related to the thermal expansion effect induced by heat release in the main jet. As discussed in Figs. 2 and 3, different predictions on the progress of combustion in the core zone of jet have been made by the nonpremixed and premixed flamelet simulations. Concerning the fluctuating velocity U_d'', far from the centerline, the computed values tend to exceed the experimental data. However, the present LES calculation shows a better agreement than that obtained in the RANS simulation [52], in which the velocity fluctuations are underpredicted owing to the inadequate estimation of turbulent intensity. Similar observations on the overestimation of droplet fluctuating velocity were made in other LES studies [6,39]. The predicted higher temperature and the enhanced evaporation associated with it could have caused this discrepancy. The consideration of an adequate dispersion model is also expected to improve the results since the overprediction can be a result of insufficient droplets near the flame edge for obtaining the spray statistics.

4.1.3. Reaction zone

As discussed above, the combustion chemistry described by diffusion and premixed flamelets leads to different flame structures in terms of the gas temperature and spray evaporation. In this

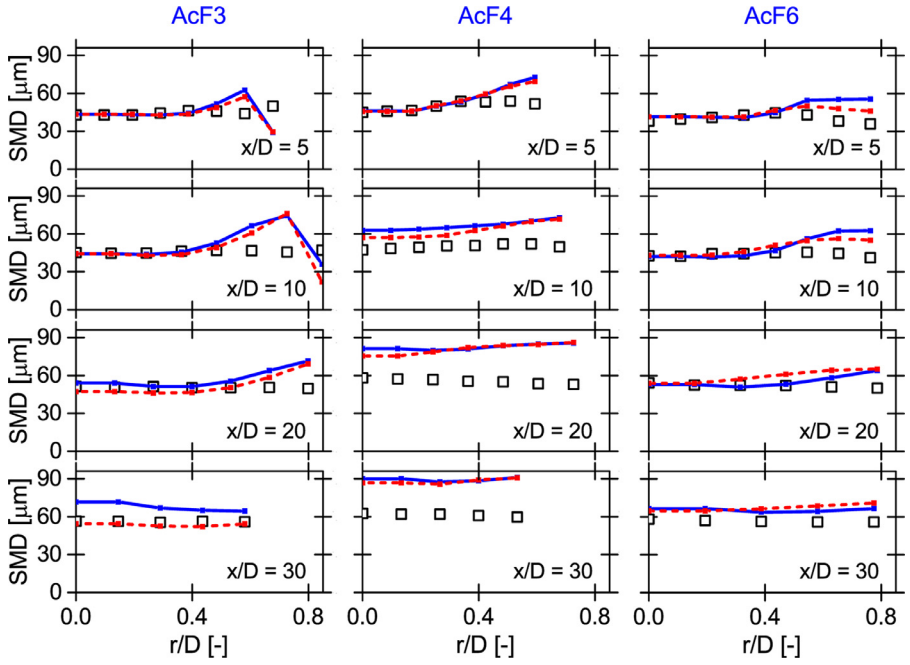

Fig. 4. Comparison of Sauter mean diameter (SMD) predicted by nonpremixed and premixed flamelet simulations with experimental data for spray flames AcF3 (left), AcF4 (middle) and AcF6 (right) at four axial locations of x/D = 5, 10, 20, and 30. Solid line: nonpremixed flamelet calculations; Short dash: premixed flamelet calculations; Dots: experimental data [29].

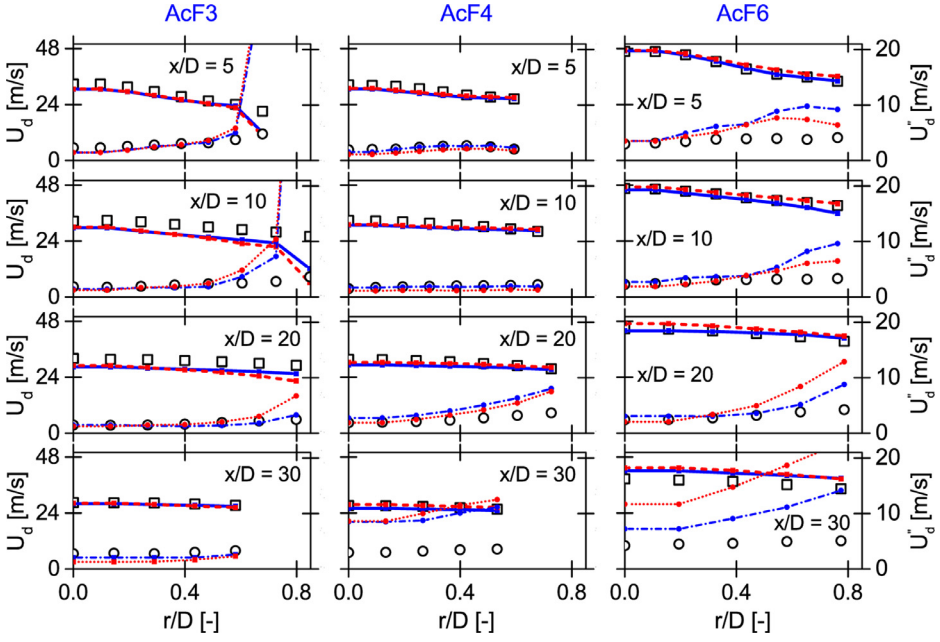

Fig. 5. Comparison of droplet mean and fluctuating axial velocity U_d, U_d'' predicted by nonpremixed and premixed flamelet simulations with experimental data for spray flames AcF3 (left), AcF4 (middle) and AcF6 (right) at four axial locations of x/D = 5, 10, 20, and 30. Solid and dash-dot lines: nonpremixed flamelet calculations; Short dash and dot lines: premixed flamelet calculations; Square: measured data of U_d; Circle: measured data of U_d'' [29].

section, the reaction mode is explored to further analyze the key mechanism.

Figure 6 illustrates the instantaneous field of reaction rate overlapped with the isoline of gas temperature $T = 738$ K in AcF6 predicted by the two flamelet calculations. Firstly, as expected, it is noted that in the two figures the isoline of $T = 738$ K, which is the ignition temperature of the acetone/air mixture, generally embraces the region in which the main reaction occurs. The high-temperature reaction zone initiated from the reactive pilot developed with increasing distance from the exit plane through either the coflow entrainment or ignition of central premixed fuel mixture, which could be delayed or prompted by the evaporation. On the other hand, it is seen that the combustion reaction in these two flamelet computations shows significantly different patterns. The premixed flamelet computes two evident areas of reaction on either side of the pilot-stream which are mainly attached to the flow interface between the pilot with main jet and coflow. In comparison, the nonpremixed flamelet leads to a more widely

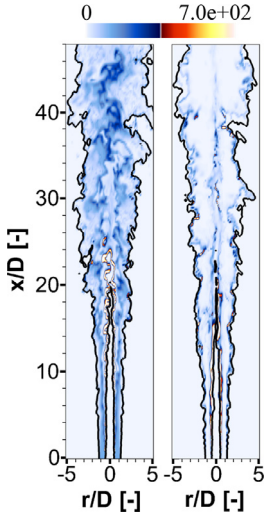

Fig. 6. Snapshots of the reaction rate predicted by nonpremixed (left) and premixed (right) flamelet simulations of spray flame AcF6. Black solid line: isoline of gas temperature with value of 738 K.

distributed reaction. Comparisons are also conducted for two other test flames (not shown here), where a similar observation is obtained.

Figure 7 shows scatter plots of gas-phase temperature, T against the equivalence ratio, ϕ for the three test flames obtained by using the nonpremixed (top) and premixed (bottom) flamelet. The samples in the plots are collected from all the filter cells at the across-section $x/D = 10$. In general, a closed circle formed by the scatters is observed in the $T-\phi$ map, which substantially differs from the one that would be observed in the gaseous flames operated using a similar piloted burner [53]. Comparatively, a cluster of scatter data exists on the rich-side of the flame ($\phi > 1$) that varies with temperature and equivalence ratio, which is created mainly by spray evaporation in the central jet. Depending on the distance from the piloted reacting front, fuel droplets show a different degree of evaporation. The fuel pockets left by the evaporation then mix with the oxidiser and form a core domain of stratified combustible gases characterised by an increasing temperature with the increase of equivalence ratio. For a given value of equivalence ratio, a number of scatters with a slowly rising reaction rate are observed, corresponding to a premixed burning mode. This premixed propagating layer heading towards the inner unburnt core zone persists till the base of flame near the centerline is established at the downstream. In the case of AcF4 with a nonpremixed flamelet model, since the inner flame front is formed further upstream as shown in Fig. 2, its scatter plot shows fewer scatter data at the fuel-rich side (see the figure at top-middle).

In accordance with the observation in Fig. 6, in the premixed flamelet, two apparent reaction zones are found, and the stoichiometric mixtures ($\phi = 1$) in the pilot stream stay in the equilibrium state with a negligible reaction rate, in contrast to the nonpremixed flamelet case, which shows intense reaction. It is also worth noting that, on the lean side, the premixed flamelet starts the reaction at approximately $T = 1100$ K compared to $T = 550$ K in case of diffusion flamelet, which may explain the higher predicted temperature in this lean region ($r/D > 1$) by the diffusion flamelet, as shown in Fig. 3.

In flamelet simulations, the chemistry properties are determined from the flamelet lookup table through the solved mixture fraction, Z, and progress variable, C, which include the effect of turbulent transport or chemical reactions and spray evaporation. Illustrated in Fig. 8 is the general distribution of the computed mixture fraction and progress variable in the flow field of the three spray flames, which is displayed in terms of the iso-contour of joint normalized histogram of Z and C. The difference between the solid and dash-dot-dot lines in the figures is that the latter takes into account the samples only in the central fuel stream.

The contour shows two main regions with significant variations of Z and C. The first region, with a low progress variable in the A part, corresponds to the evolution of premixed jet mixtures at the center flow. The second, referred to as the B zone, featuring a high C and a broader range of mixture fraction around the stoichiometric value Z_{st}, associates with the mixing layer around the

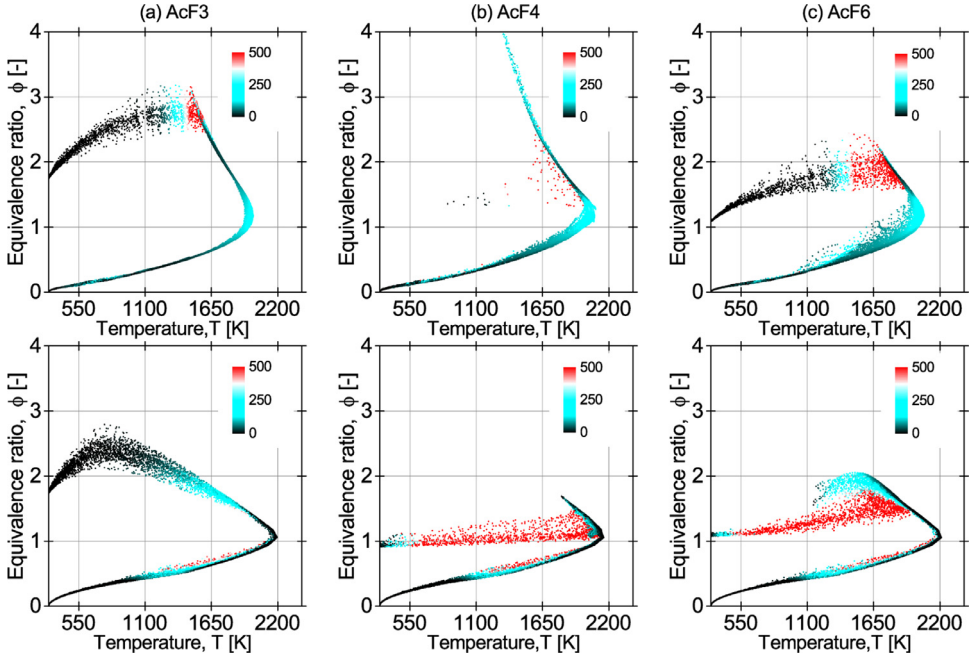

Fig. 7. Scatter plots of the gas temperature vs. equivalence ratio obtained in nonpremixed (top) and premixed (bottom) flamelet simulations of spray flames AcF3, AcF4 and AcF6 at cross-section x/D = 10. Dots are colored with the reaction rate.

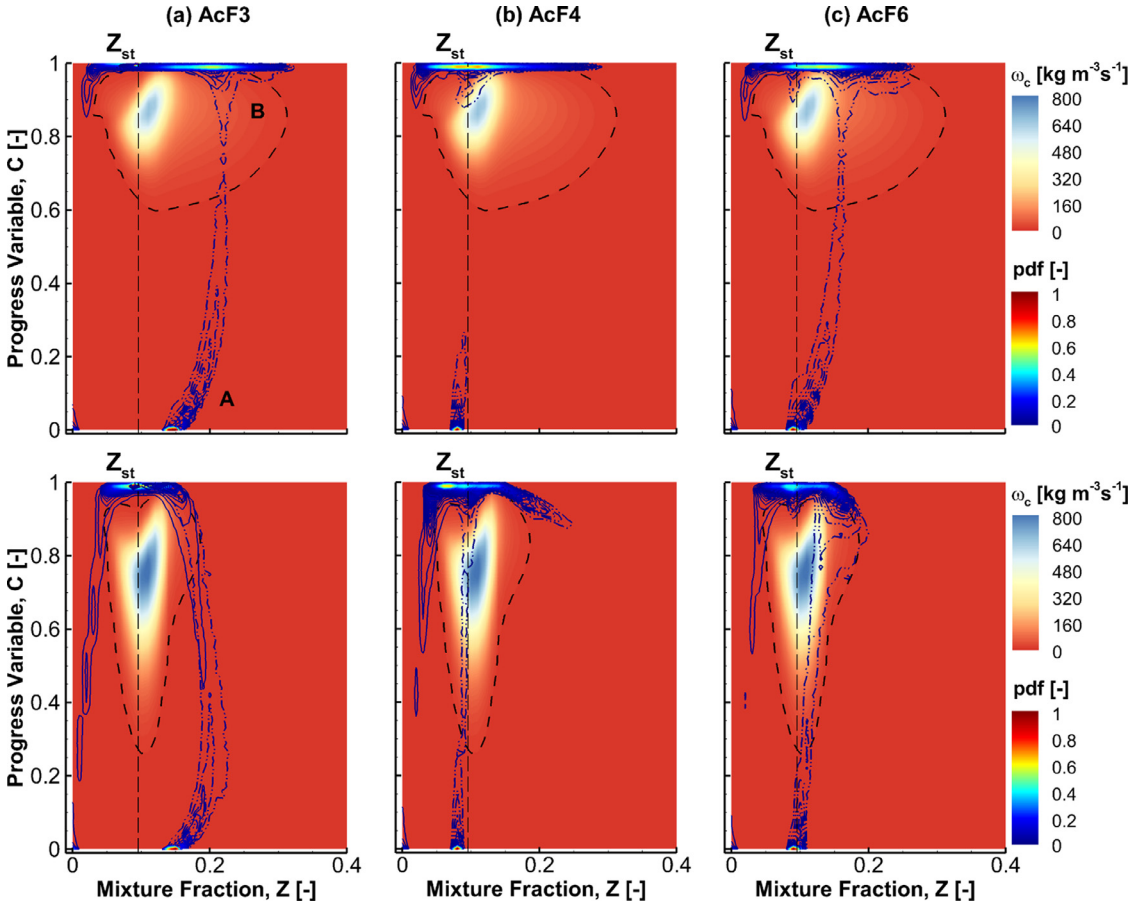

Fig. 8. Iso-contours (solid and dash-dot-dot lines) of joint normalized histogram of mixture fraction, Z against progress variable, C obtained in nonpremixed (top) and premixed (bottom) flamelet calculations of three test flames, which are overlaid with the contours of reaction rate determined from the corresponding flamelet libraries. Thick dash line indicates the region with significant reaction rate. Vertical dash line: location of stoichiometric mixture fraction Z_{st}.

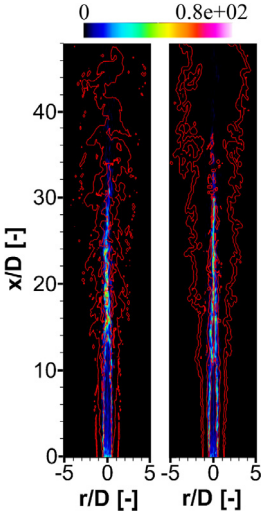

Fig. 9. Instantaneous field of spray evaporation rate for spray flame AcF6 from the simulations with nonpremixed (left) and premixed (right) flamelet. The overlapped solid-lines denote locations of the intense reaction region marked by $Y_{OH} \times Y_{CH_2O}$.

pilot stream. In the three flames investigated here, the mixture fractions at the inlet determined based on the pre-vaporized fuel and air flow rate listed in Table 1 are 0.146 (AcF3), 0.08 (AcF4) and 0.094 (AcF6), which are reflected on the different initial points with $C = 0$ in the A region for the three flames. Starting from this initial premixed mixture, the spreading of possible reactant states towards the upper region in $Z - C$ space confirms the mixing processes between the streams of main jet and hot pilot when moving farther downstream. Owing to the evaporative fuel addition in the spray jet, a curved spreading domain, indicating this two-stream interaction, is observed instead of a straight domain that connects upper and lower regions directly which would be expected in gaseous flames with only the dominant effect of turbulent mixing. In the B zone, a two-wing structure appears. The lean branch delineates the entrainment of air coflow to the reacting mixture of the pilot, while at the rich side, the premixed mixtures end up fully burnt through a combustion trajectory affected by the initial condition, droplet evaporation and turbulence.

In AcF3, as illustrated in the temperature profile of Fig. 3, the premixed flamelet shows an underpredicted temperature near the axis region compared to the values obtained from the diffusion flamelet and the experiments. The central flow temperature is linked to the evolution trajectory of part A, as shown here for AcF3. In the premixed case, the contour of reaction rate has a narrow inverted-triangle distribution, and due to the lack of diffusion in the Z direction for the area with low C, the evaporated fuel experiences the inadequately predicted reaction progress rate. Near the nozzle exit, the burning rate in the central flow is more like diffusion controlled. Thus, the heat transfer between the neighboring mixed fuel/air pockets in this region is not taken into account properly by the premixed flamelet database. Nevertheless, when one moves downstream, even the nonpremixed flamelet leads to a higher prediction of gas temperature, which indicates that no

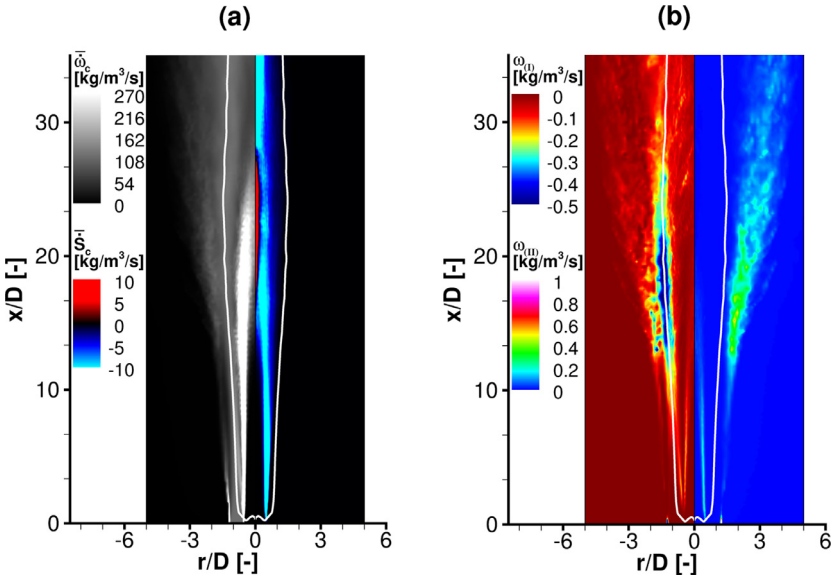

Fig. 10. Contours of source terms in progress variable Eq. (8) from nonpremixed flamelet calculations of AcF6. (a): reaction rate $\bar{\dot{\omega}}_c$ (left) and spray source term $\bar{\dot{S}}_c$ (right); (b): source terms of $\omega_{(I)}$ (left) and $\omega_{(II)}$ (right), respectively. White solid line: isoline of stoichiometric mixture fraction.

single-regime flamelet that is derived from the scenario of asymptotic premixed or nonpremixed flames can appropriately simulate the spray combustion. Spray flames under consideration, as discussed in the subsequent section, are characterized by a structure of evaporation-dominant reaction zones, presenting both nonpremixed and premixed behavior.

It should be also noted that in AcF4 under the lean condition, the reaction path of spray jet mixtures initialized in the A zone tends to reach upwards of the stoichiometric condition in the B side through a straight line since AcF4 has the smallest liquid mass loading at inlet among the three cases. Hence, the effect of spray evaporation is not apparent in AcF4 with a small increment of mixture fraction for unburnt central gases. Comparatively, AcF6 has a similar amount of inlet premixed reactant but a much higher liquid injection rate, resulting in the rich combustion of the central fresh mixture in B zone with a curved reaction path. This explains why the inner flame front starts earlier in AcF4 than in AcF6 as has been revealed in Fig. 2. If the spray effect is neglected for AcF6, its combustion trajectory would be similar to that observed in AcF4, where the central jet mixes quickly with the stoichiometric burning mixture in the pilot. This implies that evaporating droplets can change the chemical structures of the flame significantly and leave distinct footprints in the $Z-C$ space.

4.2. Spray-reaction interaction

As demonstrated in above discussions, the accurate prediction of spray flames is affected by the representative flamelet structures and the close coupling with sprays needs to be accounted for with care. In this work, a form of the C governing equation newly derived for two-phase flows is employed, accounting for the influence of spray/reaction interaction, a further analysis of which is given below based on the predictions resulting from the two different flamelet simulations of case AcF6 with the highest liquid mass loading, and a similar observation can be made for two other spray cases.

Figure 9 shows the pattern of spray evaporation interacting with intense reaction regions (indicated by the isoline of $Y_{OH} \times Y_{CH_2O}$) in the nonpremixed (left) and premixed (right) flamelet simulations of AcF6. As can be seen in the case of nonpremixed flamelet simulation, the inner reaction zone occurs in the shear layer which is directed inwards the central jet, where the hot pilot transfers the heat to the spray mixture, promoting droplet evaporation close to the layer interface. In turn, the evaporation fuels the reaction zone for further expansion. With increasing downstream distance, the central jet breaks down around $x/D = 15$, following which combustion reaction establishes at the axis region and subsequently enhances the interaction of the reaction with upcoming sprays. For the premixed flamelet case, the reaction at the inner side tends to be broader in space interacting with central sprays. This can be related to the fact that premixed flamelet structures contain information regarding the species and heat fluxes in progress variable space, promoting the propagation of the reaction zone to the lower C area, which can be observed in Fig. 8. Overall, in both nonpremixed and premixed flamelet computations, the evaporating sprays show a pronounced interaction with reaction, even though different patterns are observed.

To investigate the influence of spray effects on the reaction progress, the contour of source terms in the two-phase C Eq. (8) is shown in Figs. 10 and 11. When a nonpremixed flamelet is considered, as displayed in Fig. 10, it can be seen that the dominant area of spray evaporation of $\bar{\dot{S}}_c$ overlaps with the intense reaction zone of $\bar{\dot{\omega}}_c$ in space, and in most areas especially within the inner shear layer, the evaporation tends to decrease the local combustion intensity with a negative $\bar{\dot{S}}_c$ and to slow the progress of reactants to achieve equilibrium. A similar observation is made for the premixed flamelet calculation in Fig 11 except for the broader interaction zone for the spray and reaction. As for the terms of $\omega_{(I)}$ and $\omega_{(II)}$, they are not spray related, showing their main distribution out of the area where the interaction of spray/reaction dominates. The term $\omega_{(I)}$ associated with $d^2Y_c^{eq}/dZ^2$ presents a local maximum with a negative value along the stoichiometric line, and it contributes mainly to flamelet reaction in a diffusion mode [32]. On the other hand, $\omega_{(II)}$ remains small with a positive value compared to $\omega_{(I)}$. Note that the model used in this work for the cross-dissipation rate $\tilde{\chi}_{Z,C}$ in $\omega_{(II)}$ may lead to the overestimation of $\tilde{\chi}_{Z,C}$ [54]. Thus, it can be deduced that the influence of $\omega_{(I)}$ and $\omega_{(II)}$ is negligible in the present flames. However, as noted by Bray et al. [32], this may need reconsideration in a partially premixed flame, where flame propagation is highly affected by the closely coupled Z and C fields with a steeper gradient.

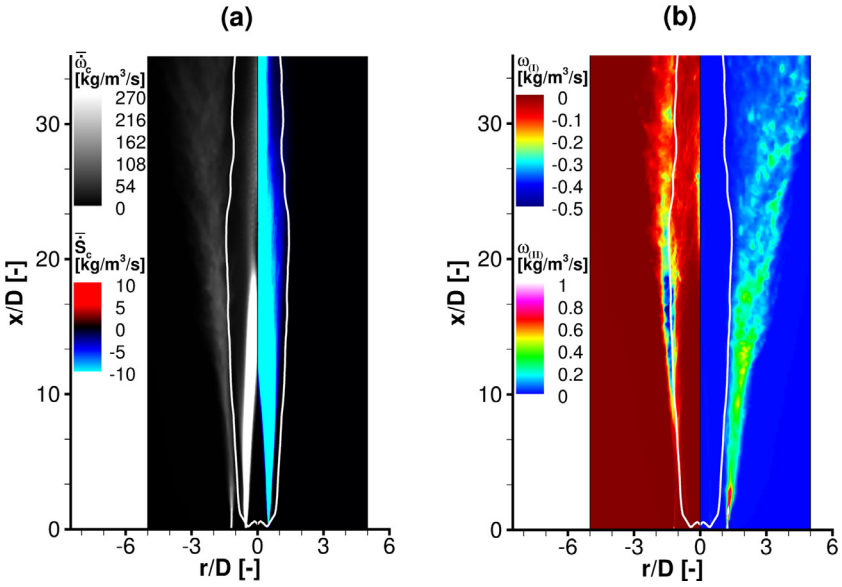

Fig. 11. Contours of source terms in progress variable Eq. (8) from premixed flamelet calculations of AcF6. (a): reaction rate $\bar{\dot{\omega}}_c$ (left) and spray source term $\bar{\dot{S}}_c$ (right); (b): source terms of $\omega_{(I)}$ (left) and $\omega_{(II)}$ (right), respectively. White solid line: isoline of stoichiometric mixture fraction.

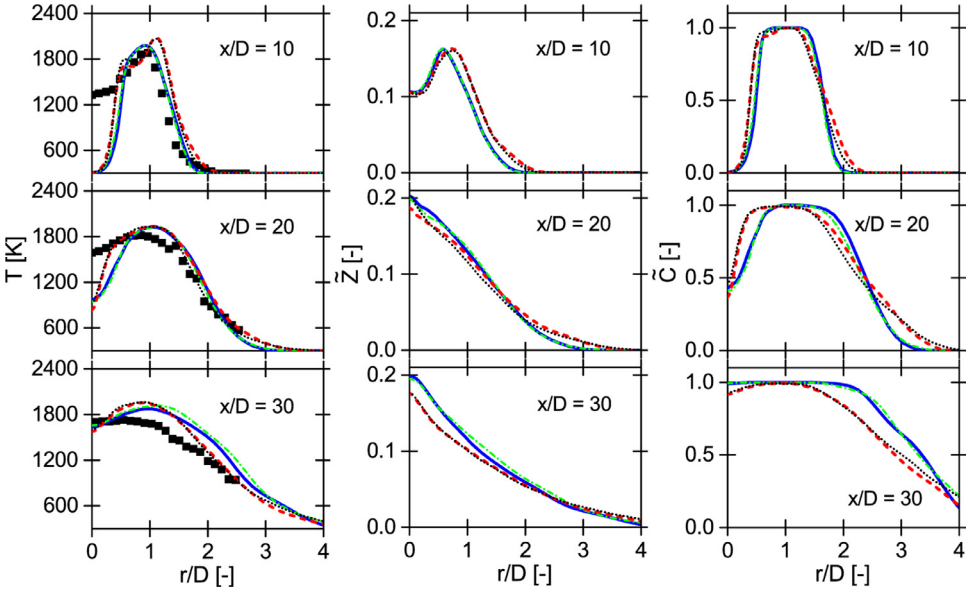

Fig. 12. Comparison of radial profiles of mean gas temperature (left), mixture fraction (middle) and progress variable (right) computed for case AcF6. Solid ——— and dash-dot _·_ lines denote, respectively, the computations from nonpremixed flamelet with and without the consideration of source term $\bar{\dot{S}}_c$. Dash - - - and dot ···· lines denote, respectively, the computations from premixed flamelet with and without the consideration of source term $\bar{\dot{S}}_c$. Dots: experimental data only available for temperature [29].

Plotted in Fig. 12 are the radial profiles of gas-phase temperature, mixture fraction and progress variable computed by use of two different flamelet chemistries for AcF6. The computations that neglect the spray source term $\bar{\dot{S}}_c$ in the C equation are included for comparison. It can be seen that the profile of the progress variable is shifted slightly outwards in the calculations with the spray source term, which can be linked to the observed suppression effect of evaporating sprays on the reaction zone (see e.g., Figs. 10 and 11). The inward flame propagation is delayed when considering the spray source term, and a subsequent smaller temperature profile is found at the downstream position $x/D = 30$. Consistent with the observations made on the mean values, the results of RMS gas temperature shown in Fig. 13 also indicate that the cases considering spray source term tend to predict a decreased temperature fluctuations. The reaction intense in combustion region is affected by the source term in C equation, and because of the dissipation effect of droplets the gas phase RMS temperature declines accordingly. Since the spray source term is only included in the filtered transport equation of mean progress variable, the predicted RMS of mixture fraction and progress variable shows a small sensitivity to the spray effects. As indicated in the work of De et al. [28] by considering spray terms in equation of SGS variance of Z, the spray evaporation can be important in the lean cases of Sydney spray flames. The same study can be carried out for the progress variable variance by deriving a corresponding two-phase equation of $\widetilde{C''}$, which will not be discussed in this study. In general a small effect of $\bar{\dot{S}}_c$ on the flamelet predictions is observed in the dilute spray configuration considered here.

It is worth noticing that the new spray source term $\bar{\dot{S}}_c$ serves to be the scalar fluxes driven by spray in flamelet subspace. It has a

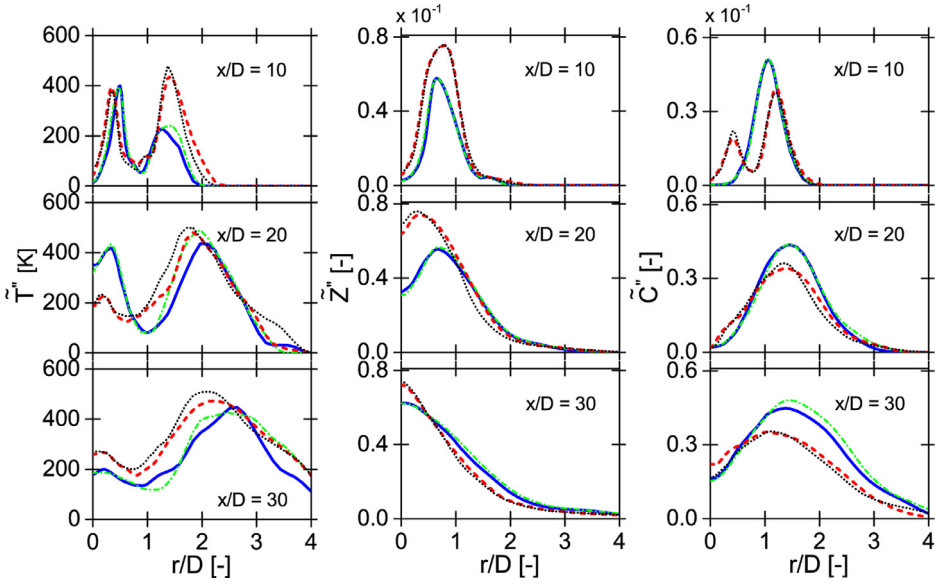

Fig. 13. Comparison of radial profiles of RMS gas temperature (left), mixture fraction (middle) and progress variable (right) computed for case AcF6. Solid ___ and dash-dot _·_ lines denote, respectively, the computations from nonpremixed flamelet with and without the consideration of source term $\bar{\dot{S}}_c$. Dash - - - and dot .... lines denote, respectively, the computations from premixed flamelet with and without the consideration of source term $\bar{\dot{S}}_c$.

similar form as that found in the spray flamelet equation of species mass fraction derived by Olguin and Gutheil [4] as $S_v(Z-1)\frac{\partial Y_i}{\partial Z}$. There, in a configuration of counterflowing spray flame, it was observed that this source term arising from evaporation can dominate the transport equation of products with a considerable contribution to the dissipation. This is consistent with the findings of the present work, and given that $\bar{\dot{S}}_c$ is one order of magnitude smaller than $\bar{\dot{\omega}}_c$ in this flame, a more apparent effect on chemical reactions is expected for the implementation in dense sprays.

4.3. Combustion regime

In the above sections, it was shown that the chemical structures of spray flames can not be well captured by accessing a single flamelet database from either the nonpremixed or premixed flamelet method. Below, the combustion regime in this piloted spray flame is analyzed, and the calculations from the nonpremixed flamelet modeling of the three test flames are discussed.

For the investigation of flame structures, the flame index is a useful tool, which is usually determined as the normalized product of mass fraction gradient of fuel and oxidizer [55]

$$\Theta = \nabla Y_{\mathrm{Fuel}} \cdot \nabla Y_{\mathrm{O2}} / |\nabla Y_{\mathrm{Fuel}}||\nabla Y_{\mathrm{O2}}|$$

In correspondence with the premixed-like and diffusion-like reaction regime, Θ takes a positive and negative value, respectively, and its value locates within the region of $(-1,1)$.

The centerline distribution of mean temperature and mass fraction of fuel and oxygen, as well as the evaporation rate and flame index shown in Fig. 14 reveals that there exist three combustion domains marked by *a, b* and *c*, where the diffusion and partially premixed flame structures are coupled with the evaporation-dominated regime. In the *a* region, the jet flow is more evaporation dictated, featuring a small temperature but a slow increase of fuel mass fraction. The evaporation of injected droplets is driven by the initial momentum difference between the spray and gas carrier and partly by the heating effect of the pilot stream, while the heat diffused from the pilot is offset in a large part by the heat loss because of droplet evaporation. When moving far away from the nozzle exit, once the flow temperature starts to escalate with a dramatic decrease of Y_{O2}, the transition to the *b* region of a

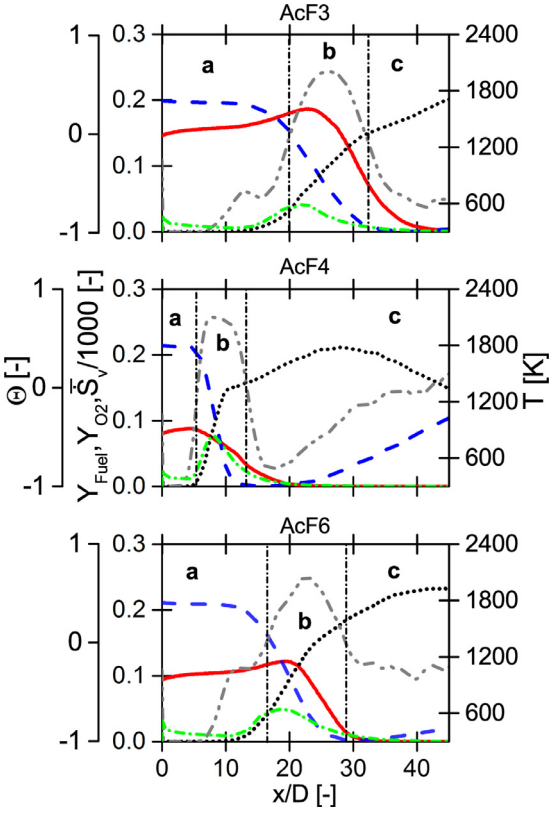

Fig. 14. Axial distribution of mean mass fraction of fuel (solid line) and oxygen (dash line), mean temperature (dot line), spray evaporation term $\bar{S}_v/1000$ (dash-dot line) as well as flame index Θ (dash-dot-dot line) along the centerline for spray flames AcF3, AcF4 and AcF6.

premixed-type flame is observed and the flame index increases from negative to the positive value. The droplets in the core region of the jet begin to evaporate faster and outstrip the consumption of fuel in the preheat zone, leading to the continuous increase of Y_{Fuel}, which differs from the gaseous premixed flames. In a later

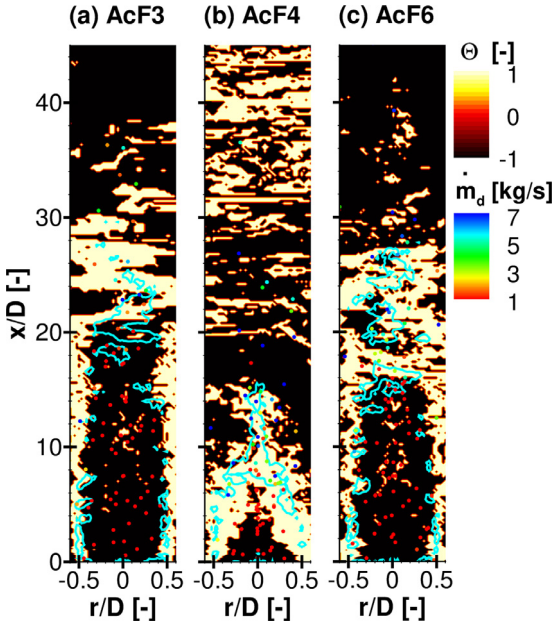

Fig. 15. Contour of flame index near the axis region. Isoline —— indicates the spray region with significant evaporation. Filled dots: representative droplets in the flow field colored by their individual evaporate rate.

stage, Y_{Fuel} experiences a big slump resulting from the establishment of the main premixed burning zone near the centerline. Further downstream, the diffusion flame in the *c* domain develops along with a declining negative flame index because of the leakage of fuel from the *b* region and the oxidizer entrained from coflow. In terms of temperature profiles, a dual-reaction structure is observed, particularly in lean flame AcF4, with two peaks at downstream locations corresponding to the partially premixed flame and a subsequent diffusion flame. It is also observed that the evaporation rate increases promptly when sprays reach the vicinity of premixed flame front in *b* domain, although a relatively high evaporation is also found close to the inlet due to the slip velocity between the injected droplets and the turbulent flow.

For further understanding the distribution of different combustion regimes, the contour of flame index overlaid with the isoline of a region with significant evaporation is illustrated in Fig. 15. It is clear that mixed burning regimes exist in this spray flame, and they are placed closely in space, forming multilayer coupled flame structures. Apart from the middle part of the flame zone in a premixed-type indicated by the positive Θ, an evaporation-controlled regime and diffusion flame burning are found at the near- and far-field areas. Close to the inlet, owing to the accumulated vapor fuel from droplets evaporating in a relatively low temperature condition, a negative Θ is assigned to the evaporation regime, which reaches its intense region at the base of premixed flame.

This multi-regime reaction in spray flame presents a significant challenge for the predictive capability of modeling based on classical single-regime flamelet methods. Knowing this, one research effort proposed a combined implementation of both nonpremixed and premixed flamelets in a single simulation by identifying the local combustion mode with flame index and reasonable results were obtained in the simulations of gas flames [16,23,31]. As indicated in this work, however, the simple form of Θ can fail to differentiate the evaporation-dominated regime from the diffusion burning since they could hold the same negative Θ. Another attempt resorts to the establishment of a model flamelet configuration that fits the spray case, where the inherent spray effect on flamelet structures is incorporated in the tabulated chemistry. This includes the spray flamelet approach [56], where the flamelet structures, obtained from a counterflow diffusion spray flame, well predicted the turbulent spray flames controlled by evaporation and nonpremixed combustion. An extension of this model was attained in [26] when a partially premixed spray flame accounting for the pre-vaporization effect was considered for spray flamelet generation, but its performance for various spray and gas conditions needs further validation.

In summary, for spray flames a more comprehensive flamelet-based approach should recognize the coexistence of diffusion-like and premixed-like reactions and should be able to include the regime with significant impact on chemical structures due to the spray evaporation.

5. Conclusions

Large eddy simulations of partially premixed spray flame were performed with detailed chemistry effects included by use of flamelet-based combustion models. A new formulation of the progress variable *C* equation for two-phase flows was developed and used, and it includes a spray source term in contrast to the gaseous counterpart. The single-regime nonpremixed and premixed flamelets parameterized by the mixture fraction and progress variable were both adopted, and their performance in LES of partially premixed spray flames and dependency on the spray effect when including the proposed two-phase *C* equation were examined. The dilute spray phase was modeled in a Lagrangian way, and the SGS fluctuation effect on the evaporation was incorporated by a refined stochastic approach. The computations were discussed and compared with experiments of the Sydney reacting acetone sprays, which range from rich and lean to stoichiometric operating conditions.

It was found that two flamelet predictions considering the source term of progress variable generally showed a good agreement with the measurements in terms of gas temperature, droplet size, and velocity. Yet a marked difference between nonpremixed and premixed flamelet calculations was observed. Generally, the premixed flamelet captured the downstream jet spreading in the radial direction while overestimating the peak temperature compared to the non-premixed chemistry. The diffusion flamelet, on the other hand, yielded an earlier combustion for central premixed spray mixtures. The disagreement between two flamelet simulations tends to become small in the stoichiometric flame. The reason for this difference is due to the difference of reaction propagation in the mixture fraction and progress variable subspace indicated by these two flamelet models. The analysis of $Z-C$ histograms showed that apart from the effect of diffusion and chemical reaction, evaporating droplets add another free dimension affecting the combustion trajectory of premixed reactants in the core jet, which in turn influences the stabilization of inner flame front. Thus, these Sydney spray flames characterize a hybrid combustion regime, where combustions occurring in diffusion-like and premixed-like regimes are closely located in space and strongly coupled by the turbulent transport and spray evaporation. The present study indicated that the single-regime flamelet can not fully describe the spray flames, and a more reliable modeling would rely on the flamelet structures that should recognize the multi-regime reactions interacted with evaporating sprays.

It was also found that the new spray source term $\bar{\dot{S}}_c$ in the *C* equation is identified to act as an important scalar flux induced by spray evaporation in flamelet structures and thus the incorporation of $\bar{\dot{S}}_c$ can potentially play an important role in the predictive capabilities of flamelet models. In the present calculations of turbulent spray flame, it contributed mainly to the retardation of chemical

reactions and slow down the flame propagation towards the inner jet. In both nonpremixed and premixed flamelet simulations, the major impact area of $\bar{S}_c$ overlaps with the area of main reaction regime. Although its effect on the chemical reactions is small in the present dilute sprays, a future study on its implementation in dense sprays is warranted.

Acknowledgments

This research was partially supported by MEXT (Ministry of Education, Culture, Sports, Science, and Technology) as ″ Priority issue on Post-K computer″ (Accelerated Development of Innovative Clean Energy Systems), and by MEXT Grant in Aid (No.16H04278). Y.H. thanks Prof. A.R. Masri at the University of Sydney for providing the experimental measurements.

Appendix A. Transport equation of reaction progress variable for reacting spray flows

For the flamelet-based tabulation technique, the species mass fraction Y_i can be expressed directly in terms of the mixture fraction Z and progress variable C as

$$Y_i(\mathbf{x},t) = Y_i[Z(\mathbf{x},t), C(\mathbf{x},t)] \tag{37}$$

The formulations for the temporal and spatial derivatives of $Y_i(\mathbf{x}, t)$ can then be written as

$$\partial_t Y_i = \partial_Z Y_i \partial_t Z + \partial_C Y_i \partial_t C, \tag{38}$$

$$\nabla Y_i = \partial_Z Y_i \nabla Z + \partial_C Y_i \nabla C. \tag{39}$$

By multiplying Eqs. (38) and (39) with the gas density ρ and mass flux $\rho\mathbf{u}$, respectively, and combining the resulting equations, after rearranging terms, we obtain

$$\rho\frac{\partial C}{\partial t} + \rho\mathbf{u}\cdot\nabla C = \left(\rho D_t Y_i - \rho D_t Z\frac{\partial Y_i}{\partial Z}\right)\cdot\frac{1}{\partial Y_i/\partial C}, \tag{40}$$

where $D_t = \partial_t + \mathbf{u}\cdot\nabla$ is the substantial derivative.

The use of the governing equations of the species mass fraction Y_i and the mixture fraction Z for multiphase flows

$$\rho\frac{\partial Y_i}{\partial t} + \rho\mathbf{u}\cdot\nabla Y_i = \nabla\cdot(\rho\alpha\nabla Y_i) + \dot{\omega}_i + \dot{S}_{Y_i} - Y_i\dot{S}_v \tag{41}$$

$$\rho\frac{\partial Z}{\partial t} + \rho\mathbf{u}\cdot\nabla Z = \nabla\cdot(\rho\alpha\nabla Z) + \dot{S}_v - Z\dot{S}_v, \tag{42}$$

in the above derived equation for the progress variable C, Eq. (40), yields

$$\rho\frac{\partial C}{\partial t} + \rho\mathbf{u}\cdot\nabla C = \left(\rho\alpha\nabla^2 Y_i + \dot{\omega}_i + \dot{S}_{Y_i} - Y_i\dot{S}_v\right)\frac{1}{\partial Y_i/\partial C} - \frac{\partial Y_i}{\partial Z}\left(\rho\alpha\nabla^2 Z + \dot{S}_v - Z\dot{S}_v\right)\frac{1}{\partial Y_i/\partial C}. \tag{43}$$

On the right hand side, S_v is the mass source term associated with vaporization. S_{Y_i} is the production rate of species Y_i due to evaporation processes. For the single component spray droplets, S_{Y_i} is zero except in the case of $Y_i = Y_{fuel}$. $\dot{\omega}_i$ is the chemical reaction rate. Here, the assumption of a constant diffusion coefficient α is adopted. Y_i can denote the mass fraction of a single species or a sum of multiple species; for the latter case, the assumption of equal diffusion coefficients for all species considered is additionally used to ensure the same form of Eq. (41).

The progress variable C in a normalized form is usually defined by [31,32]

$$C = Y_i(\mathbf{x},t)/Y_i^{eq}(Z(\mathbf{x},t)) \tag{44}$$

with $Y_i^{eq}(Z(\mathbf{x},t))$ being the corresponding equilibrium value of species mass fraction and being a function of only the mixture fraction Z, which implies

$$\frac{\partial Y_i}{\partial C} = Y_i^{eq}, \quad \frac{\partial^2 Y_i}{\partial C^2} = 0$$
$$\frac{\partial^2 Y_i}{\partial C\partial Z} = \frac{dY_i^{eq}}{dZ}, \quad \frac{\partial^2 Y_i}{\partial Z^2} = C\frac{d^2 Y_i^{eq}}{dZ^2} \tag{45}$$

By Inserting of the following formulation of $\nabla^2 Y_i$

$$\frac{\partial}{\partial x_i}\left(\frac{\partial Y_i}{\partial x_i}\right) = \frac{\partial}{\partial x_i}\left(\frac{\partial Y_i}{\partial C}\frac{\partial C}{\partial x_i} + \frac{\partial Y_i}{\partial Z}\frac{\partial Z}{\partial x_i}\right) = \frac{\partial Y_i}{\partial C}\frac{\partial^2 C}{\partial x_i^2} + \frac{\partial Y_i}{\partial Z}\frac{\partial^2 Z}{\partial x_i^2} + \frac{\partial^2 Y_i}{\partial C^2}\left(\frac{\partial C}{\partial x_i}\right)^2 + \frac{\partial^2 Y_i}{\partial Z^2}\left(\frac{\partial Z}{\partial x_i}\right)^2 + 2\frac{\partial^2 Y_i}{\partial C\partial Z}\frac{\partial C}{\partial x_i}\frac{\partial Z}{\partial x_i} \tag{46}$$

and Eq. (45) into Eq. (43), the transport equation of the progress variable C for spray flows can finally be reformulated to

$$\partial_t(\rho C) + \nabla\cdot(\rho\mathbf{u}C) - \nabla\cdot(\rho\alpha\nabla C) = \left[\dot{\omega}_i + C\frac{d^2 Y_i^{eq}}{dZ^2}\rho\chi_Z + 2\frac{dY_i^{eq}}{dZ}\rho\chi_{Z,C}\right]\frac{1}{Y_i^{eq}} - \left[C\frac{dY_i^{eq}}{dZ}(\dot{S}_v - Z\dot{S}_v)\right]\frac{1}{Y_i^{eq}}, \tag{47}$$

the last term of which represents the source term derived from the effects of spray vaporization. $\chi_Z = \alpha|\nabla Z|^2$ and $\chi_{Z,C} = \alpha\nabla Z\cdot\nabla C$ are the scalar dissipation rate of mixture fraction and the cross-dissipation term, respectively.

References

[1] Y. Baba, R. Kurose, Analysis and flamelet modeling for spray combustion, J. Fluid Mech. 612 (2008) 45–79.
[2] P. Jenny, D. Roekaerts, N. Beishuizen, Modeling of turbulent dilute spray combustion, Prog. Energy Combust. Sci. 38 (2012) 846–887.
[3] M.S. Raju, On the importance of chemistry/turbulence interactions in spray computations, Numer. Heat. Tr. B-Fund. 41 (2002) 409–432.
[4] H. Olguin, E. Gutheil, Influence of evaporation on spray flamelet structures, Combust. Flame 161 (2014) 987–996.
[5] S. Ukai, A. Kronenburg, O.T. Stein, LES-CMC of a dilute acetone spray flame, Proc. Combust. Inst. 34 (2013) 1643–1650.
[6] A. Rittler, F. Proch, A.M. Kempf, LES of the sydney piloted spray flame series with PFGM/ATF approach and different sub-filter models, Combust. Flame 162 (2015) 1575–1598.
[7] E. Abtahizadeh, L.P.H. De Goey, J.A.V. Oijen, LES of delft jet-in-hot coflow burner to investigate the effect of preferential diffusion on autoignition of CH4/h2 flames, Fuel 191 (2017) 36–45.
[8] N. Patel, S. Menon, Simulation of spray-turbulence-flame interactions in a lean direct injection combustor, Combust. Flame 153 (2008) 228–257.
[9] V.N. Prasad, A.R. Masri, S.N. Martinez, K.H. Luo, Investigation of auto-ignition in turbulent methanol spray flames using large eddy simulation, Combust. Flame 160 (2013) 2941–2954.
[10] Y. Pei, E.R. Hawkes, S. Kook, G.M. Goldin, T. Lu, Modelling n-dodecane spray and combustion with the transported probability density function method, Combust. Flame 162 (2015) 2006–2019.
[11] X. Jiang, G. Siamas, K. Jagus, T. Karayiannis, Physical modelling and advanced simulations of gas– liquid two-phase jet flows in atomization and sprays, Prog. Energy Combust. Sci. 36 (2010) 131–167.
[12] S.B. Pope, Small scales, many species and the manifold challenges of turbulent combustion, Proc. Combust. Inst. 34 (2013) 1–31.
[13] A. Giusti, E. Mastorakos, Detailed chemistry LES/CMC simulation of a swirling ethanol spray flame approaching blow-off, Proc. Combust. Inst. 36 (2017) 2625–2632.
[14] N. Peters, Laminar diffusion flamelet models in non-premixed turbulent combustion, Prog. Energy Combust. Sci. 10 (1984) 319–339.
[15] M. Ihme, H. Pitsch, Prediction of extinction and reignition in nonpremixed turbulent flames using a flamelet/progress variable model. 2. application in LES of Sandia flames d and, E, Combust. Flame 155 (2008) 90–107.
[16] B. Fiorina, O. Gicquel, L. Vervisch, S. Carpentier, N. Darabiha, Approximating the chemical structure of partially premixed and diffusion counterflow flames using FPI flamelet tabulation, Combust. Flame 140 (2005) 147–160.
[17] J.A. van Oijen, L.P.H. de Goey, Modelling of premixed laminar flames using flamelet-generated manifolds, Combust. Sci. Technol. 161 (2000) 113–137.

[18] E. Knudsen, Shashank, H. Pitsch, Modeling partially premixed combustion behavior in multiphase LES, Combust. Flame 162 (2015) 159–180.
[19] H.A. EI-Asrag, A.C. Iannetti, S.V. Apte, Large eddy simulations for radiation-spray coupling for a lean direct injector combustor, Combust. Flame 161 (2014) 510–524.
[20] S. Tachibana, K. Saito, T. Yamamoto, M. Makida, T. Kitano, R. Kurose, Experimental and numerical investigation of thermo-acoustic instability in a liquid–fuel aero-engine combustor at elevated pressure: validity of large-eddy simulation of spray combustion, Combust. Flame 162 (2015) 2621–2637.
[21] A.W. Vreman, B.A. Albrecht, J.A. van Oijen, L.P. de Goey, R.J.M. Bastiaans, Premixed and nonpremixed generated manifolds in large-eddy simulation of sandia flame d and f, Combust. Flame 153 (2008) 394–416.
[22] W.J.S. Ramaekers, J.A. van Oijen, L.P.H. de Goey, A priori testing of flamelet generated manifolds for turbulent partially premixed methane/air flames, Flow Turbul. Combust. 84 (2010) 439–458.
[23] P. Domingo, L. Vervisch, J. Réveillon, DNS analysis of partially premixed combustion in spray and gaseous turbulent flame-bases stabilized in hot air, Combust. Flame 140 (2005) 172–195.
[24] S. Subramaniam, Lagrangian-eulerian methods for multiphase flows, Prog. Energy Combust. Sci. 39 (2013) 215–245.
[25] C.D. Pierce, P. Moin, Progress-variable approach for large-eddy simulation of non-premixed turbulent combustion, J. Fluid Mech. 504 (2004) 73–97.
[26] Y. Hu, H. Olguin, E. Gutheil, A spray flamelet/progress variable approach combined with a transported joint PDF model for turbulent spray flames, Combust. Theory Model. 21 (2017) 575–602.
[27] J. Réveillon, L. Vervisch, Spray vaporization in nonpremixed turbulent combustion modeling: a single droplet model, Combust. Flame 121 (2000) 75–90.
[28] S. De, S.H. Kim, Large eddy simulation of dilute reacting sprays: droplet evaporation and scalar mixing, Combust. Flame, 160 (2013) 2048–2066.
[29] J.D. Gounder, A. Kourmatzis, A.R. Masri, Turbulent piloted dilute spray flames: flow fields and droplet dynamics, Combust. Flame 159 (2012) 3372–3397.
[30] D.K. Lilly, A proposed modification of the Germano subgridscale closure method, Phys.Fluids A 4 (1992) 633–635.
[31] P. Domingo, L. Vervisch, K. Bray, Partially premixed flamelets in LES of nonpremixed turbulent combustion, Combust. Theory Model. 6 (2002) 529–551.
[32] K. Bray, P. Domingo, L. Vervisch, Role of the progress variable in models for partially premixed turbulent combustion, Combust. Flame 141 (2005) 431–437.
[33] J.B. Michel, O. Colin, C. Angelberger, D. Veynante, Using the tabulated diffusion flamelet model ADF-PCM for simulating a lifted methaneair jet flame, Combust. Flame 156 (2009) 1318–1331.
[34] H. Pitsch, H. Steiner, Large-eddy simulation of a turbulent piloted methane/air diffusion flame (Sandia flame d), Phys. Fluids 12 (2000) 2541–2554.
[35] C.D. Pierce, P. Moin, A dynamic model for subgrid variance and dissipation rate of a conserved scalar, Phys. Fluids 10 (1998) 3041.
[36] P.-D. Nguyen, V. L, V. Subramanian, P. Domingo, Multidimensional flamelet–generated manifolds for partially premixed combustion, Combust. Flame 157 (2010) 43–61.
[37] M.M. Salehi, W.K. Bushe, N. Shahbazian, C.P.T. Groth, Modified laminar flamelet presumed probability density function for LES of premixed turbulent combustion, Proc. Combust. Inst. 34 (2013) 1203–1211.
[38] H. Pitsch, Flamemaster v3.1: A c++ computer program for 0d combustion and 1d laminar flame calculations, 1998.
[39] M. Chrigui, J. Gounder, A. Sadiki, A.R. Masri, J. Janicka, Partially premixed reacting acetone spray using LES and FGM tabulated chemistry, Combust. Flame 159 (2012) 2718–2741.
[40] M. Chrigui, A.R. Masri, A. Sadiki, J. Janicka, Acetone droplet behavior in reacting and non-reacting turbulent flow, Flow Turbul. Combust. 90 (2013) 813–832.
[41] L. Ma, B. Naud, D. Roekaerts, Transported PDF modeling of ethanol spray in hot-diluted coflow flame, Flow Turbul. Combust. 96 (2016) 469–502.
[42] D.C. Haworth, Progress in probability density function methods for turbulent reacting flows, Prog. Energy Combust. Sci. 36 (2010) 168–259.
[43] R.S. Miller, K. Harstad, J. Bellan, Evaluation of equilibrium and non-equilibrium evaporation models for many-droplet gas-liquid flow simulations, Int. J. Multiph. Flow 24 (1998) 1025–1055.
[44] M. Bini, W.P. Jones, Large-eddy simulation of particle-laden turbulent flows, J. Fluid Mech. 614 (2008) 207–252.
[45] T. Kitano, J. Nishio, R. Kurose, S. Komori, Effects of ambient pressure, gas temperature and combustion reaction on droplet evaporation, Combust. Flame 161 (2014) 551–564.
[46] C. Heye, V. Raman, A.R. Masri, Influence of spray/combustion interactions on auto-ignition of methanol spray flames, Proc. Combust. Inst. 35 (2015) 1639–1648.
[47] T. Kitano, K. Kaneko, R. Kurose, S. Komori, Large-eddy simulations of gas- and liquid-fueled combustion instabilities in back-step flows, Combust. Flame, 170 (2016) 63–78.
[48] T. Hara, M. Muto, T. Kitano, R. Kurose, S. Komori, Direct numerical simulation of a pulverized coal jet flame employing a global volatile matter reaction scheme based on detailed reaction mechanism, Combust. Flame 162 (2015) 4391–4407.
[49] S. Pichon, G. Black, N. Chaumeix, M. Yahyaoui, H.J. Curran, J.M. Simmie, R. Donohue, The combustion chemistry of a fuel tracer: measured flame speeds and ignition delays and a detailed chemical kinetic model for the oxidation of acetone, Combust. Flame 156 (2009) 494–504.
[50] R.W. Bilger, A mixture fraction framework for the theory and modeling of droplets and sprays, Combust. Flame 158 (2011) 191–202.
[51] M. Klein, A. Sadiki, J. Janicka, A digital filter based generation of inflow data for spatially developing direct numerical or large eddy simulations, J. Comput. Phys. 186 (2003) 652–665.
[52] Y. Hu, H. Olguin, E. Gutheil, Transported joint probability density function simulation of turbulent spray flames combined with a spray flamelet model using a transported scalar dissipation rate, Combust. Sci. Technol. 189 (2017) 322–339.
[53] M. Juddoo, A.R. Masri, S.B. Pope, Turbulent piloted partially-premixed flames with varying levels of o-2/n-2: stability limits and PDF calculations, Combust. Theory Model. 15 (2011) 773–793.
[54] S.P. Malkeson, N. Chakraborty, Statistical analysis of cross scalar dissipation rate transport in turbulent partially premixed flames: a direct numerical simulation study, Flow Turbul. Combust. 87 (2011) 313–349.
[55] H. Yamashita, M. Shimada, T. Takeno, A numerical study on flamestability at the transition point of jet diffusion flames, Symp. (Int.) Combust. 26 (1996) 27–34.
[56] C. Hollmann, E. Gutheil, Flamelet-modeling of turbulent spray diffusion flames based on a laminar spray flame library, Combust. Sci. Technol. 135 (1998) 175–192.